Design of a Soft Anthropomorphic Hand with Active Stiffness control

Submitted in partial fulfillment of the requirements

of the degree of

Bachelor of Technology and Master of Technology

by

Abhishek Sharma

(*Roll no.* 120100061)

Supervisor:

Prof. Abhishek Gupta

Mechanical Engineering

Indian Institute of Technology Bombay

2017

Dissertation Approval

This dissertation entitled **"Design of a Soft Anthropomorphic Hand with Impedance control"**, submitted by Abhishek Sharma (Roll No. 120100061), is approved for the award of degree of Bachelor of Technology and Master of Technology in Mechanical Engineering.

Examiners

Supervisor

Chairman

Date: 13..... July 2017

Place: MUMBAI

Declaration of Authorship

I declare that this written submission represents my ideas in my own words and where others' ideas or words have been included, I have adequately cited and referenced the original sources. I also declare that I have adhered to all principles of academic honesty and integrity and have not misrepresented or fabricated or falsified any idea/data/fact/source in my submission. I understand that any violation of the above will be cause for disciplinary action by the Institute and can also evoke penal action from the sources which have thus not been properly cited or from whom proper permission has not been taken when needed.

Signature: 

Abhishek Sharma
120100061

Date: 19. July 2017

Abstract

In a robotic hand it is desirable to have low mechanical and control complexity as well as the capability to perform a variety of tasks. This cannot be achieved simultaneously in the existing hand designs. In this project we present a design in which multiple finger joints are actuated using a single displacement actuator and two multiarticular tendons which apply torques at multiple joints. Compliance is introduced between the pulleys and the joints. This design allows the finger to have a structure with reduced mechanical complexity and weight. Further, this structure also results in control equations such that individual actuator behaviors can be linearly superimposed, regardless of posture. This leads to lesser control complexity. This is in contrast to other dextrous robotic hands where coupling of actuators leads to considerable control complexity. Even with simpler mechanical as well as control structure, the finger can perform a variety of tasks. For example, it can be used to implement multiple synergies, end point impedance control and trajectory tracking to name a few. Due to its built in compliance, the design is also capable of conforming to surface of the object in contact in order to establish grip. The compliance is also important from the safety standpoint as it allows the finger to yield to a certain degree in case of collision and thereby absorb the impact. Dynamic simulations highlighting these capabilities are presented in the results. We have built a prototype of the finger along with a palm, using rapid prototyping. Experiments were performed using the displacement actuator like the free motion of finger and interaction with objects of different shapes and sizes, highlighting the capability to grasp different objects and track surfaces by conforming to them as result of built-in compliance of the finger.

Contents

Chapter 1

Introduction

The aim of this project is to study ways in which robotic hands could be designed for mechanical dexterity. The inspiration for this robotic hand is the human hand itself, for the reason that it is probably one of the most dexterous gripper. Although it is the best gripper to emulate, it is extremely hard to copy even its architecture. On the skeletal side, its joints don't have have fixed axes of rotation, and rolling joints don't have simple contours. Further, these joints are actuated by tendon and muscles, whose architecture is even more complex. There are single muscles actuating a large number of joints, with a single tendon spanning multiple joints and there single joints which are actuated by simultaneous firing of several muscles. Even if the anatomy of hand is successfully copied and the role of every single muscle is understood, creating motion as human hand does in performing a simple set tasks is non-trivial. This is because it extremely hard to discern which muscles are being activated to accomplish a given task. Moreover these muscle actions don't happen at a single instant of time. They are spread over time. This gives rise to temporal overlaps of muscle activation and it's close to impossible to understand them. So, even if the architecture of hand is successfully copied, we wouldn't know how to control it effectively to perform a task.

There is evidence of morphological computations [15] in the tendon networks of human hands which implies that most of the dexterity of human hand that is ascribed to Central Nervous System is a result of the efficient mechanical architecture of human hand, as a product of evolution. Hence, while performing a grasp, the role of brain in planning the grasp may not be as pronounced. In fact, most of the related computation may be offloaded in form of morphological computation [11] by the virtue of inherent compliance of the hand and that of the interaction between object and hand.

Further, the mechanical architecture of hand, and the control architecture in the brain ensures, that there is some correlation between several degrees of freedom. This correlation is

observed in form of postural synergies[13]. While the underlying mechanism of them is not understood, synergies might be a way for the brain to cope with the complexity of controlling many degrees of freedom in real-time during daily activities. It also presents a way to reduce mechanical and control complexity of the robotic hand.

Two factors that are crucial to dexterity of hand are (i) its physical structure i.e. how links and joints are arranged, so as to form a gripper which can take several shapes and (ii) efficient control (actuation) architecture of that gripper. The former one is important because in order to perform a variety of grasps a lower bound on degrees of freedom is important. For example a human finger has three degrees of freedom to span a plan. Although it could have spanned the plane with two degrees of freedom, but its ability to curl around and enclose an object would have reduced. This points towards an efficient structure of human hand. The actuation architecture is also important in this regard as the efficient control of the hand would depend on how the actuators are used to actuate several joints. For example, with increase in the number of actuators the capability of the hand would increase but the complexity of design, size and weight of hand and also the computational complexity would increase.

Drawing inspiration from the biological hands we incorporate synergies along with multi-articular tendons to arrive at a design which has low mechanical complexity and a simple control structure. Corresponding control equations can be use to explicitly determine each of actuation parameters from the desired output. Implementing open loop control, we are able to match the desired behavior to a high degree of accuracy as we show in simulations on synergies, trajectory tracking, impedance control and disturbance rejection.

The details about the physical structure and actuation strategies commonly used in robotic hands are presented in chapter 2. Chapter 3 discusses the design of a single finger and it's control structure in detail, In chapter 4, simulation results displaying a variety of capabilities is presented and experimental results from a prototype are presented. Conclusions and future work are discussed in chapter 5.

Chapter 2

Background

2.1 Classification of Grasps by a human hand

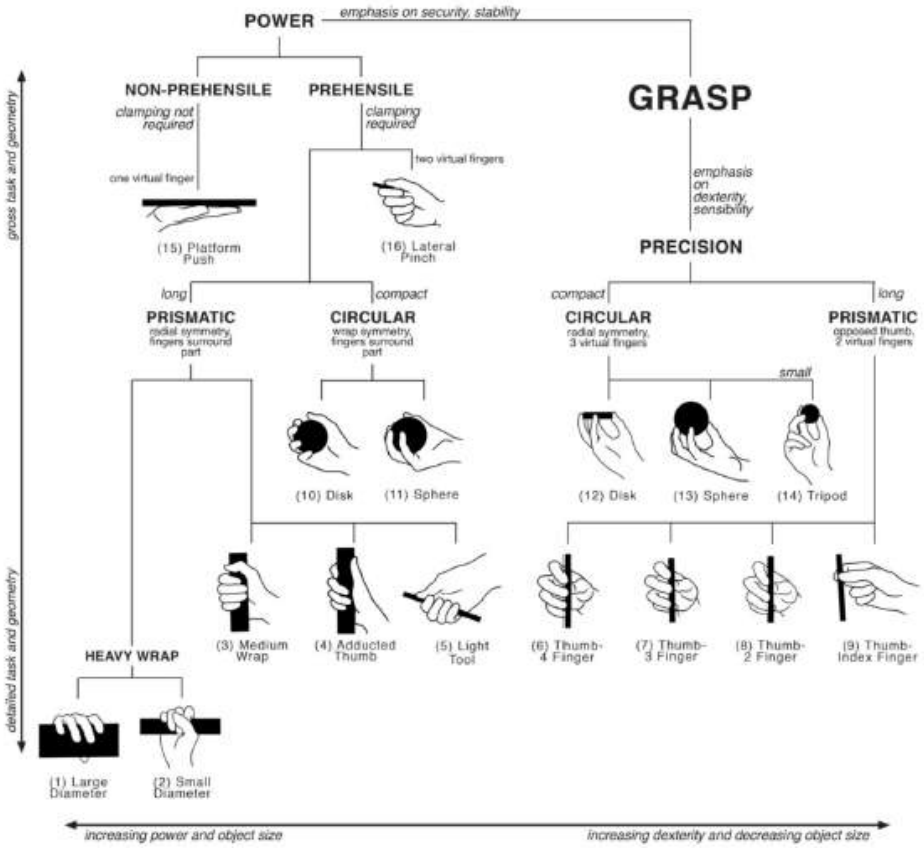

Figure 2.1: Cutkosky grasp taxonomy [6]

The Cutkosky taxonomy, shown in Fig 2.1, is currently the most widely used in the field of

robotics. The taxonomy tree is organized such that it is first divided into power and precision grasps from left to right, and by shape and function down the tree. The division between power and precision grasp is important to us when we move to whole hand design from the single finger design. This division will provide us a guideline on keeping the whole hand underactuated.

2.2 KINEMATIC MODELS USED IN ROBOTIC HANDS

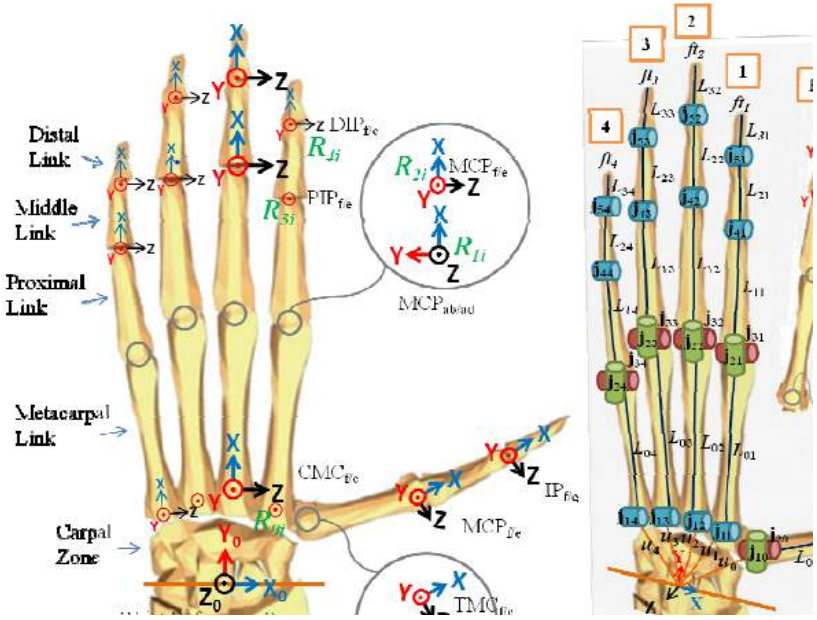

Figure 2.2: Hand Model [10]

In order to capture the kinematic capabilities of a human hand, several models for the robotic hand are used. The simplest one as shown in Fig 2.2, uses hinge joints for DIP and PIP joints while universal joint or a series of 2 hinge joints with axes perpendicular to each other to replicate the MCP joint[10]. Some hands also capture the opposition movement of the little(pinky) finger, which helps in curling the palm, to cover the object. Apart from having abduction- adduction movement for the little finger, they also have additional rotation about a tilted axis. This allows the palm to form a curvature around the object and enhance grip. Two models with this capability are shown in Fig 2.3a and Fig 2.3c. In addition to these capabilities, Pupin Hand [12] as shown in Fig 2.3b, introduces compliance between metacarpal links of Index-Middle fingers and Ring-Little fingers allowing more adaptability and conformity to the palm.

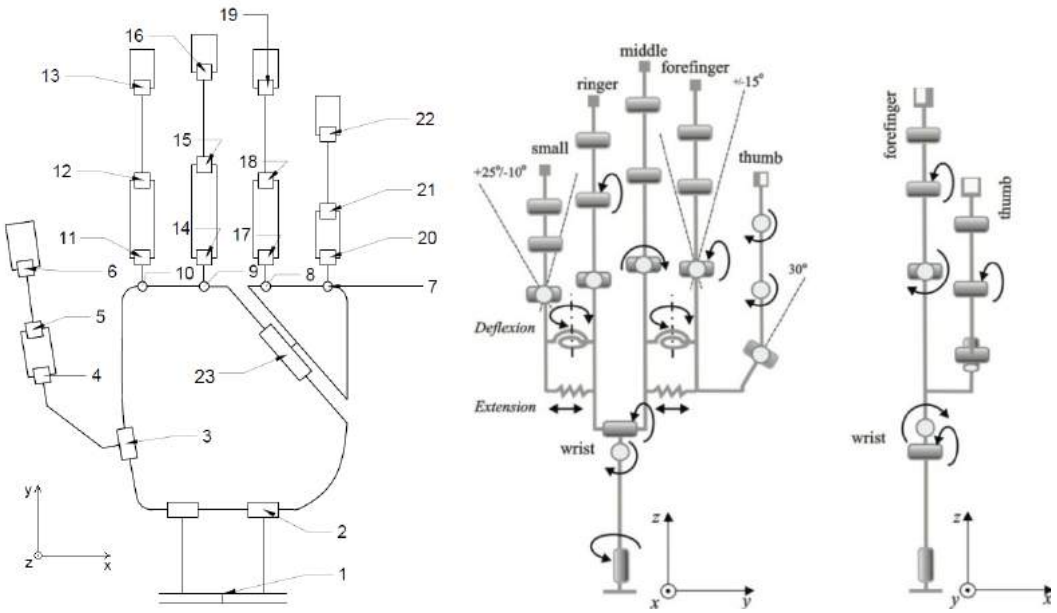

(a) Robotic Hand Model. [17]

(b) Pupin Hand Model. [12]

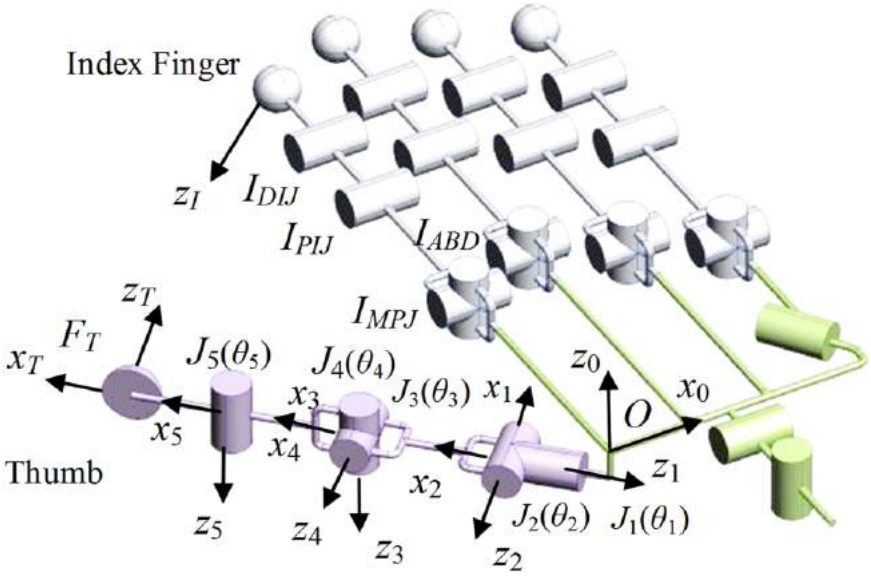

(c) Shadow Hand Model. [5]

Figure 2.3: Kinematic Models of some robotic hands

2.3 CLASSIFICATION OF ACTUATORS

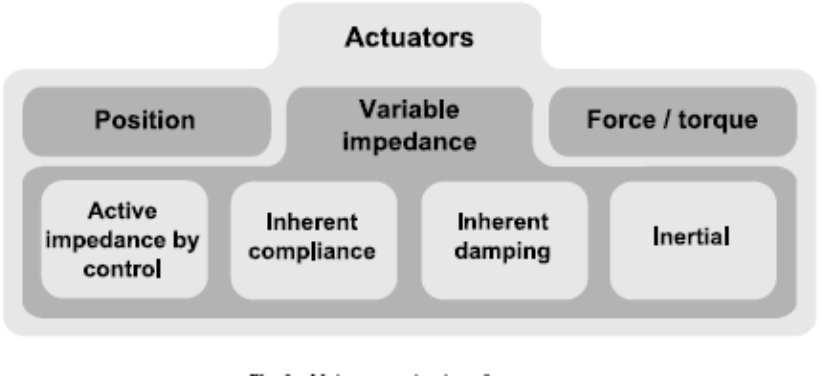

Figure 2.4: Classification of actuators. [16]

As shown in the Fig 2.4, actuators used for robotic hands can be classified into 3 primary categories: position controller, torque controller and variable impedance actuator. Position controllers (or stiff actuators) can be seen as having a very high stiffness and follow the source trajectory accurately, regardless of external forces for example servo motors. These are particularly very important for precise position control applications in industries and where uncertainty in the environment is low [16]. On the other hand, Torque controllers have zero virtual impedance and act as a force source for example direct drive motors or constant torque springs [16].
Another category of actuators, in contrast to stiff actuators is the compliant actuators which take the position depending on the equilibrium between external forces and the impedance (stiffness and damping) properties of the actuator. Compliant actuators can be further divided into 2 sub-categories:(i) constant compliance actuators(series elastic actuators) and (ii) variable compliance actuators. Compliant actuators are important from the safety point of view, for their capacity to absorb the energy in case of a collision and thus, prevent damage to the robot and human. Also, in case dynamic applications like throwing, compliant actuators have shown better performance than stiff actuators through efficient use dynamics of the system. Moreover, variable compliance actuators offer even better safety and performance advantages over constant compliance actuators.

2.3.1 Variable Impedance Actuators

Variable stiffness actuator have application in robots that must physically interact with an unknown and dynamic environment. They offer following advantages: (i) energy efficiency

e.g. in motions like throwing, walking (natural gait) (ii) ability to mimic both position control (high stiffness) and force control (low stiffness) actuators and (iii) safety.
These Actuators can be further divided based on: (i) active impedance control and (ii) passive (or mechanical) compliance.

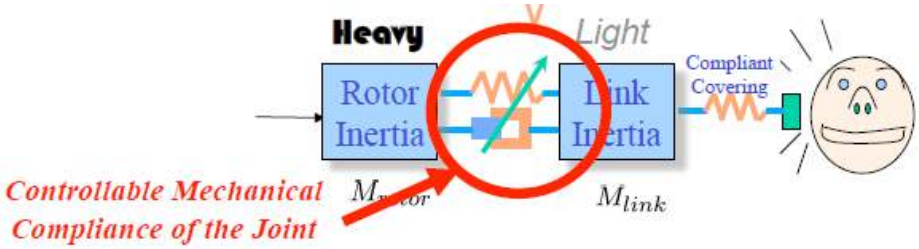

Figure 2.5: Passive Variable Compliance [1]

Passive variable compliance (see Fig. 2.5) is a category of variable impedance actuators where an actual spring and a mechanism to change its stiffness are employed. Such mechanisms are discussed in the next section.

2.3.1.1 Variable Passive Compliance Mechanism

Variable passive compliance mechanisms can be primarily classified into to two configurations: (i) antagonistic configuration and (ii) series configuration. Antagonist configurations,

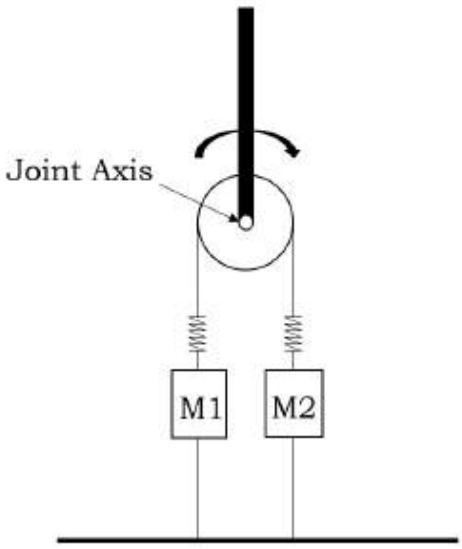

Figure 2.6: Antagonist configuration [16]

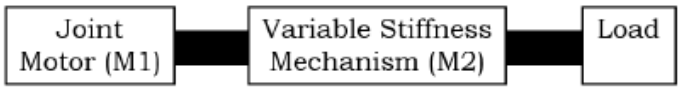

Figure 2.7: Series Configuration [16]

as shown in the Fig 2.6, use two non-linear springs. When one spring is pulled while other is released, position of the pulley is altered while if both are pulled/released simultaneously stiffness of the joint is changed. In series configurations(see Fig. 2.7) joint motor decides the position, while separate variable stiffness mechanism is used between the joint motor and link. Series configuration often use spring pre-loading, variable transmission or material properties to alter the stiffness. In spring pre-loading (Fig. 2.9), the apparent stiffness of the spring between the actuator and the link is changed by controlling the initial deflection in the spring. In case of variable transmission mechanism (Fig. 2.8), position of the spring, which determines the moment arm of the spring force, is changed to control the actuator stiffness. Antagonist mechanisms typically have low-stiffness ranges and are energetically

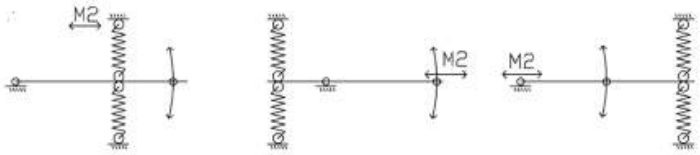

Figure 2.8: Variable Transmission in Series Passive VSA [16]

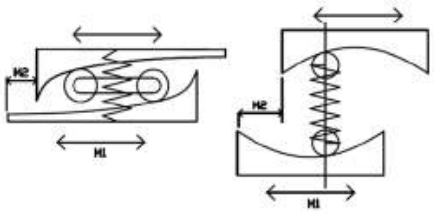

Figure 2.9: Spring Pre-loading in series Passive VSA [16]

inefficient as two motors have to be online, to maintain the stiffness. Series VSA don't have these disadvantages, but are mechanically complex and heavier.

2.3.2 Active Impedance control

Active impedance control (see Fig 2.10) involves use of stiff actuators, sensors and controller, to imitate the properties of a passive compliance actuator. However, Active Impedance

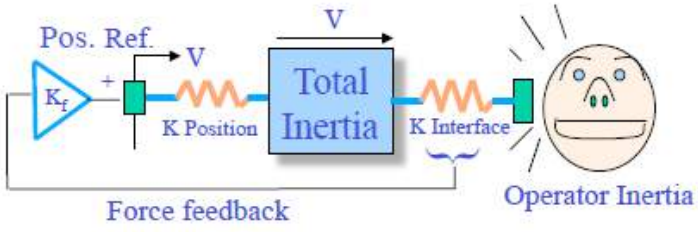

Figure 2.10: Active Impedance Control [1]

Control doesn't use any actual springs so, there is no provision to store energy and optimize energy usage. In fact, it takes energy for the system to mimic the compliance. Also, for Active Impedance Control in case of collision, detection and action play important role in safety. So, sensor and actuators are required to be fast enough. The benefit of active impedance control is that it can enable faster adjustment of stiffness as compared to passive variable actuators

2.4 Actuation Strategies

2.4.1 Full Hand Actuation

Under this scheme, as shown in Fig 2.11, every single joint is independently controlled leading to mechanical and computational complexity. This scheme is hardly used for anthropomorphic hands due to this complexity .

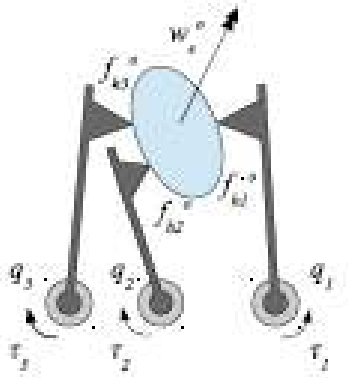

Figure 2.11: Full Hand Actuation [4]

2.4.2 Adaptive Under-Actuation

Adaptive under-actuated hands make use of an approach based on differential transmissions, which distribute the displacements of a very small number of motors to all the fingers. This is used to reduce the degrees of actuation all the while allowing the hand to adapt to the surface of object. In Fig 2.12 one can see that, if any of the link comes in the contact with a rigid object or is blocked, then the pulleys would accommodate and allow movement of unblocked joints, until they are blocked by the object. Use of this strategy in a hand allows it to maximize its contact with the object. Examples of such hands are [7] and [8].

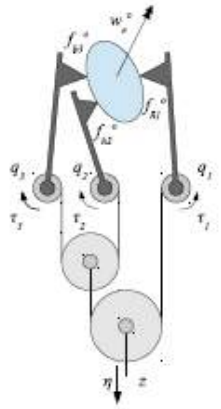

Figure 2.12: Adaptive Under-Actuation [4]

2.4.3 Synergies

Joint movements in human hand are correlated and brain appears to command the hand as a unit (depending on task) rather than individually actuated joints. This is revealed in the several studies done in neuroscience. There correlations in joint movements are referred to as kinematic synergies. Underlying factor for these observed synergies are (i) the anatomy of the hand i.e. the tendon and muscle networks, and their connection to the joints (ii) cortical control scheme underlying the activation of these muscles i.e. temporal variation in actuation of muscles. What is even more crucial is that these synergies might be a way for brain to deal with the complexity of actuating 20 dofs in real time while performing a task.
Statistical tools like Principal Component Analysis have been used to determine correlations in joint actuation during human hand movements. As shown in [13], Principal Component Analysis of a set of static hand postures, reveals that first few (3-4) eigenpostures (synergies), superimposed on each other are able to explain more than 80% of the variation in the given set of hand postures. These synergies are however task dependent. A study encompassing

even broader set of tasks [14], like unconstrained exploration, mimed grasps, actual grasps etc, has also given the evidence of existence of synergies although more number of synergies are required to explain the same variation in hand postures. Also important, is the observation that higher order synergies account for finer variations in the gross hand posture, which is obtained using first few synergies. Thus, the existence of this form of correlation in the joint movements can be exploited in simplifying the control of an anthropomorphic robotic hand.

2.4.3.1 Application of Synergies in Anthropomorphic Hand

To determine the synergies, Principal Component Analysis (PCA) is applied on the posture matrix obtained using joint angle data obtained for static hand postures corresponding to the grasps of given set of objects [2].
Each posture is represented by a vector comprising the joint angles. The vector for grasp of i^{th} object is:

$$q = P_i = \begin{bmatrix} q_1 & \dots & q_r & \dots & q_h \end{bmatrix}^T \tag{2.1}$$

The posture matrix is given by:

$$P = \begin{bmatrix} P_1 & \dots & P_s & \dots & P_n \end{bmatrix} \tag{2.2}$$

where h is the number of joints and n is the number of postures.
Using PCA on matrix P , eigenvectors E_k with corresponding eigenvalues, $\lambda_{i,k}$ are determined and any column P_i, of the given posture matrix P can be expressed as:

$$q = P_i = \sum_{k=1}^{h} a_{i,k} E_k = S \cdot a_i \tag{2.3}$$

where, $a_{i,k}$ is some constant dependent on the posture matrix and

$$S = \begin{bmatrix} E_1 & \dots & E_s & \dots & E_h \end{bmatrix} \qquad and \qquad a_i = \begin{bmatrix} a_{i,1} & \dots & a_{i,s} & \dots & a_{i,h} \end{bmatrix}^T \tag{2.4}$$

Of the h eigenvectors, only the r which have the greatest eigenvalues are used to reconstruct the approximate hand postures:

$$q \approx q_\sigma = a_{i,1} E_1 + a_{i,2} E_2 + \dots\dots\dots + a_{i,r} E_r \tag{2.5}$$

Replacing $a_{i,k}$ by σ_k to obtain any general posture from these eigenvectors, the equation becomes:

$$q_\sigma = \sigma_1 E_1 + \sigma_2 E_2 + ... + \sigma_r E_r = q_\sigma = E \cdot \sigma \tag{2.6}$$

where

$$E = \begin{bmatrix} E_1 & ... & E_s & ... & E_r \end{bmatrix} \qquad and \qquad \sigma = \begin{bmatrix} \sigma_1 & ... & \sigma_s & ... & \sigma_r \end{bmatrix}^T \tag{2.7}$$

For example using two synergies (r=2) with h=20 (human hand) the posture equation becomes:

$$q_\sigma = \sigma_1 E_1 + \sigma_2 E_2 = \sigma_1 \begin{bmatrix} E_{1,1} \\ E_{2,1} \\ . \\ . \\ . \\ E_{20,1} \end{bmatrix} + \sigma_2 \begin{bmatrix} E_{1,2} \\ E_{2,2} \\ . \\ . \\ . \\ E_{20,2} \end{bmatrix} \tag{2.8}$$

By changing the values of σ_1 and σ_2, different postures can be obtained. Hence, they can be interpreted as actuators. The actuators can be used to either input displacement or force.

2.4.3.2 Displacement based synergies

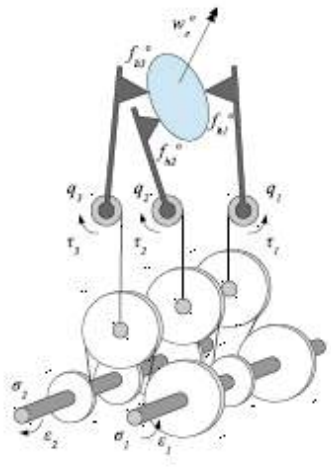

Figure 2.13: Displacement Synergies [4]

In displacement synergy, the actuation variable is motor displacement. One way to implement this is shown in [2] where σ_1 and σ_2 are rotations of shaft connected to the motor

and $E_{j,k}$ is the diameter of the pulley corresponding to actuation of j^{th} joint on the k^{th} shaft. Contributions from two shafts are added as shown in Fig.2.13. This way each joint gets contribution from the two synergies represented by the two shafts. Ratio of pulley diameters on one shaft represent the corresponding eigenvector. Thus, we get joint angles as a function of two actuation variable, in the form given in eqn (2.8) . This scheme has no compliance in it and is called Rigid Synergy [4].

2.4.3.3 Force based synergies

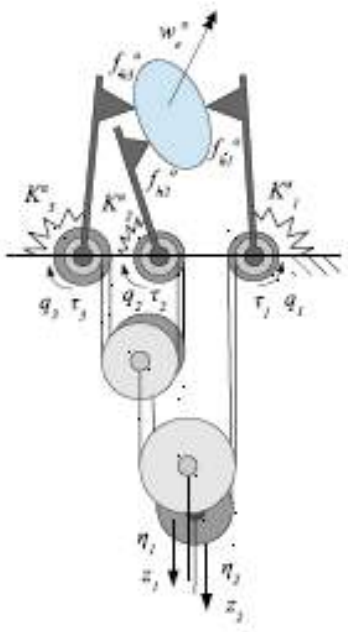

Figure 2.14: Force Synergies [4]

Fig. 2.14 shows a method of implementation of force based synergies such that σ_1 and σ_2 are actuator forces and $E_{j,k}$ is the compliance of j^{th} joint and the radius of pulley associated to the joint. Contributions from two actuators are added by addition of torques divided by the compliance of the joint from both actuators.

$$q_\sigma = \sigma_1 E_1 + \sigma_2 E_2 = C \cdot (\tau_1 + \tau_2) = F_1 \begin{bmatrix} R_{1,1}/k_1 \\ R_{2,1}/k_2 \\ . \\ . \\ R_{20,1}/k_{20} \end{bmatrix} + F_2 \begin{bmatrix} R_{1,2}/k_1 \\ R_{2,2}/k_2 \\ . \\ . \\ R_{20,2}/k_{20} \end{bmatrix} \tag{2.9}$$

Where C is the compliance matrix and k_j is stiffness associated with j_{th} joint. Also, $\sigma_k = F_k$. This scheme has inherent compliance in it and is called Adaptive Synergy, as it adapts to take the shape of the object [4].

2.4.3.4 Rigid Synergies vs Compliant Synergies

Displacement based implementation of synergy shown in Fig. 2.13 is rigid (tendons are inextensible). This poses a disadvantage because if a single joint is obstructed in its motion, other joints also lock-up. Since the hand is underactuated due to use of only a few synergies, the hand postures which need higher order synergies for their description are unattainable. Hence, use of rigid synergies for an underactuated hand could lead to ineffective grasps for some objects.
On the other hand, the force synergy shown in Fig. 2.14 is compliant, which solves the problem of joint locking. This increases the grasp quality by increasing the contact between object and hand.This can be implemented, even with use of a single actuator (first synergy) and yet the hand would establish an effective grasp. Moreover, Compliant synergies turn problem of position control into that of force control. While posture of hand is decided by the shape of the object, contact force can be controlled as shown in the next section.
Hence, compliant synergies have two-fold advantage over Rigid Synergies in terms of grasp behavior: (i) it allows establishment of better contact between object and hand, (ii) it allows control over grasp forces.
Rigid synergies have been implemented in the hand by [2]. The use of adaptive synergy is made in IIT-PISA soft hand [3]. Hand design based on adaptive synergies allow effective whole hand grasps with simple control. A single synergy is used to achieve these grasps but manipulation would require design to include higher order synergies. Stiffness changing mechanism isn't there in the hand. Also, Grasp of very thin objects is reported to be difficult.

2.4.3.5 Grasp Force control using compliant synergies

Torque acting at the j^{th} joint due to compliance of the hand is given by:

$$\tau_j = k_j(q_{j,\sigma} - q_j) \tag{2.10}$$

where, k_j is the stiffness, $q_{j,\sigma}$ is the synergistic joint angle(joint angle in case of no contact), q_j is the actual joint angle, of the j^{th} joint.

The torque matrix for entire hand is given by:

$$\tau = K \cdot (q_\sigma - q) \tag{2.11}$$

where K is the joint stiffness matrix, q is the column vector of actual joint angles.
Torques due contact forces exerted by the object on the hand are balanced by the torque generated by joint compliance, as in the following equation:

$$J^T f = \tau = K \cdot (q_\sigma - q) \tag{2.12}$$

where J and f are jacobian matrix and contact force matrix respectively, corresponding to hand-object interaction. Thus, controlling the q_σ matrix gives control over grasp forces. Also, the hand follows the synergistic trajectory, if no external contact forces are acting on the hand (f=0). (Internal friction is assumed to be absent.)
Using $q_\sigma = E \cdot \sigma$ from eqn.(2.6)

$$J^T f = \tau = K \cdot (E \cdot \sigma - q) \tag{2.13}$$

2.4.4 Variable Stiffness Actuation

Variable stiffness actuation can be done by two methods: using impedance control or using variable passive compliance actuators. Both of these have been discussed in the section 2.3. Here we present one of applications in robotic hands. One of the implementations of

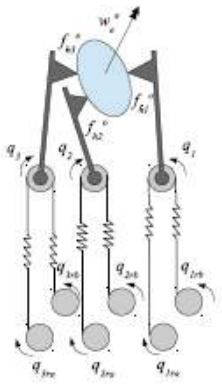

Figure 2.15: Full Variable Stiffness Actuation [4]

variable stiffness actuators is in DLR robotic hand which uses full variable stiffness actuation (see Fig. 2.15). This scheme uses antagonistic pair configuration (see Fig. 2.6) to control

stiffness for each joint. In this configuration two motors are required for each joint and so twice the number of actuators as the number of joints. This allows the ability to control the stiffness of every joint in the hand allowing greater dexterity than any other scheme. However the mechanical complexity is extremely high and so is computational complexity requiring control of a large number of actuators. Synergy can be implemented using software to reduce some of the control complexity[9]. In the DLR hand shown in Fig. 2.16 , the metacarpal joint is a hyperboloidally shaped saddle joint and interphalangeal joints are hinge joints. Joint are actuated using complex tendon network, with antagonistic variable stiffness actuation mechanism. It is designed to mimic human hand with high accuracy and also for safety under collisions.

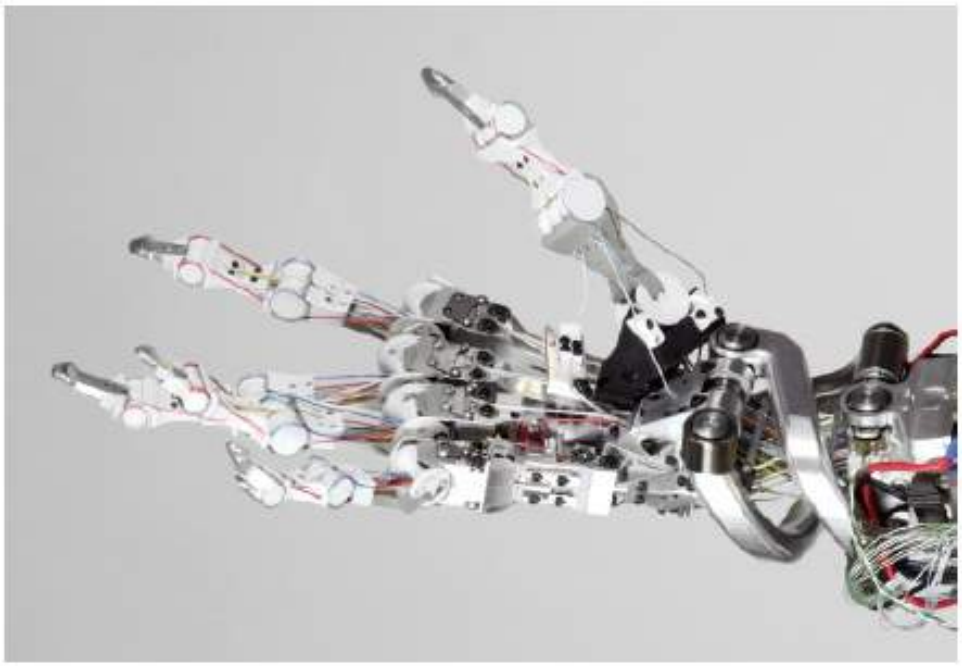

Figure 2.16: DLR Hand [9]

2.5 SUMMARY

In this chapter, we saw some of the kinematic hand models used in existing robotic hands. We also saw various types of actuators and actuation strategies used. Dexterous robotic hands like DLR which use variable stiffness actuation have very high mechanical as well as control complexity due to their large number of actuators and complex control equations. On the other hand some simpler hand designs like PISA hand use synergy and compliance to attain a simple control structure and mechanical design. However, they are limited in their capability to perform a variety of task. We try to combine synergy framework with variable stiffness actuation to arrive at a design that has a simple control and mechanical structure and it capable of a variety of tasks.

Chapter 3

Design

3.1 Finger Model

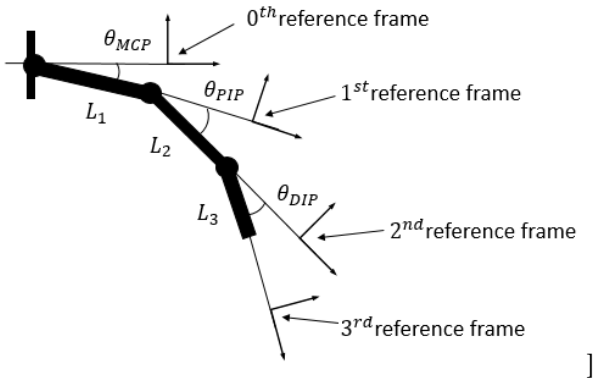

]

Figure 3.1: Finger Model.

Fig. 3.1 shows the basic finger model, with three links and three revolute joints, abduction-adduction degree of freedom has been neglected for the sake of simplicity. Each joint has an inherent stiffness and damping. How the stiffness is introduced, is discussed in the section 3.3. Dynamic equations for the finger can be derived using Euler-Lagrange equations. The position vectors for the center of masses corresponding to the phalanxes are determined. Using these corresponding velocities and kinetic energies can be computed. Potential energies corresponding to gravity and joint spring can be computed. Further, Rayleigh dissipation function can be computed using the joint velocities and damping coefficient. Neglecting abduction-adduction, the dynamic equations for a single finger are derived here. Following change of coordinates is employed: x-y is the local frame notation, while X-Y is the ground frame notation.

$$Let, \qquad \psi_1 = \theta_{MCP}; \qquad \psi_2 = \theta_{MCP} + \theta_{PIP}; \qquad \psi_3 = \theta_{MCP} + \theta_{PIP} + \theta_{DIP} \tag{3.1}$$

The position vector of center of mass of j^{th} phalanx with respect to j^{th} reference frame is given by

$$\vec{G_{jj}} = \begin{bmatrix} b_{jx} & b_{jy} & 0 \end{bmatrix}^T \tag{3.2}$$

The position vector w.r.t. the 0^{th} reference frame is given by

$$\vec{G_j} = \begin{bmatrix} G_{jx} \\ G_{jy} \\ G_{jz} \end{bmatrix} = \sum_{q=1}^{j-1} \begin{bmatrix} L_q c\psi_q \\ L_q s\psi_q \\ 0 \end{bmatrix} + \begin{bmatrix} b_{jx} c\psi_j - b_{jy} s\psi_j \\ b_{jx} s\psi_j + b_{jy} c\psi_j \\ 0 \end{bmatrix} \tag{3.3}$$

$$\vec{V_j} = \frac{d\vec{G_j}}{dt} = \dot{\vec{G}_j} \tag{3.4}$$

Total potential energy is given by

$$U = \sum_1^3 (m_j g G_{jy} + \frac{1}{2} k_j (\psi_j - \psi_{j-1})^2 \tag{3.5}$$

Total kinetic energy is given by

$$T = \frac{1}{2} \sum_1^3 (m_j V_j^2 + I_j \dot{\psi}_j^2) \tag{3.6}$$

Rayleigh dissipation function is given by

$$f = \sum_1^3 \left(\frac{1}{2} \beta_j (\dot{\psi}_j - \dot{\psi}_{j-1})^2 \right) \tag{3.7}$$

Euler-Lagrange equations in terms of generalized coordinates ψ_j :

$$\frac{d}{dt} \left(\frac{\partial (T-U)}{\partial \dot{\psi}_j} \right) - \frac{\partial (T-U)}{\partial \psi_j} + \frac{\partial f}{\partial \dot{\psi}_j} = \tau_j \tag{3.8}$$

Generalized force, τ_j can be computed using the principle of virtual work.

$$\tau_j = \frac{\sum_1^3 \delta W_j}{\delta \psi_j} \tag{3.9}$$

If a force $\vec{F} = \begin{bmatrix} F_{jx} & F_{jy} & 0 \end{bmatrix}^T$ (in local frame) is applied at the j^{th} phalanx at a point

with position vector $\vec{e}_j = [e_{jx}; e_{jy}; 0]^T$ in the j^{th} reference frame, then:

$$\tau_j = (F_{jy}e_{jx} - F_{jx}e_{jy}) + \sum_{q=j+1}^{3} \begin{bmatrix} -L_j s\psi_j \\ L_j c\psi_j \\ 0 \end{bmatrix}^T \begin{bmatrix} (F_{qX}c\psi_q - F_{qY}s\psi_q) \\ (F_{qX}s\psi_q + F_{qY}c\psi_q) \\ 0 \end{bmatrix} \tag{3.10}$$

The complete dynamic equation for the system is of the form:

$$M \begin{bmatrix} \ddot{\psi}_1 \\ \ddot{\psi}_2 \\ \ddot{\psi}_3 \end{bmatrix} + C \begin{bmatrix} \sum_{i=1}^{2} \dot{\psi}_i * \sum_{i=1}^{3} \dot{\psi}_j \\ \sum_{i=1}^{2} \dot{\psi}_i * \sum_{i=1}^{3} \dot{\psi}_j \\ \sum_{i=1}^{2} \dot{\psi}_i * \sum_{i=1}^{3} \dot{\psi}_j \end{bmatrix} + \beta \begin{bmatrix} \dot{\psi}_1 \\ \dot{\psi}_2 \\ \dot{\psi}_3 \end{bmatrix} + K \begin{bmatrix} \psi_1 \\ \psi_2 \\ \psi_3 \end{bmatrix} + G = \begin{bmatrix} \tau_1 \\ \tau_2 \\ \tau_3 \end{bmatrix} \tag{3.11}$$

where $\beta = \begin{bmatrix} \beta_1 + \beta_2 & -\beta_2 & 0 \\ -\beta_2 & \beta_2 + \beta_3 & -\beta_3 \\ 0 & -\beta_3 & \beta_3 \end{bmatrix}$, $K = \begin{bmatrix} k_1 + k_2 & -k_2 & 0 \\ -k_2 & k_2 + k_3 & -k_3 \\ 0 & -k_3 & k_3 \end{bmatrix}$,

& $M = M(\psi_1, \psi_2, \psi_3)$, $C = C(\psi_1, \psi_2, \psi_3)$, $G = G(\psi_1, \psi_2, \psi_3)$

3.2 USE OF VARIABLE COMPLIANCE IN A SOFT HAND WITH SYNERGISTIC CONTROL

Synergistic control with use of variable stiffness mechanism for joints hasn't yet been used in any robotic hand and it could have substantial advantages over constant compliance synergies.

In eqn. (2.12) the stiffness matrix K, represents the constant mechanical compliance of the joints. While the use of constant compliance makes the grasp stable for some cases, in other cases grasp may not turn out to be stable. Inherent in the adaptive synergies is thee tendency to adapt to the shape of the object. So, other types of grasps may not be possible, although this problem could be dealt with, by choosing appropriate stiffness for the joints. Moreover, the ability to control the grasp force isn't completely independent from the posture of the hand.

To deal with this, we introduce another column vector Δ in eqn (2.12) to get:

$$\tau = K \cdot (q_\sigma - q) + \Delta \tag{3.12}$$

Here Δ is torque due to additional actuators (other than synergy actuators). The implementation of these additional actuators is discussed in the design section. This allows better control

over hand postures as well as grasp forces. For example, if it is desired for the hand to hold the object in the posture such that $q_\sigma = q$ then

$$\tau = \Delta = J^T f \tag{3.13}$$

So, grasp forces can be controlled, while holding the synergistic posture ($q_\sigma = q$).This is similar to rigid synergies, only with better force control. This is similar to active impedance control. However this also increases the number of actuators. So a mechanism needs to designed with constraints on the number of actuators and mechanical complexity of the system.

3.3 DESIGN

3.3.1 Single Finger Design

In this section, the design of a single finger consisting of three joints, first synergy actuator and two stiffness controllers is presented.Two actuators are used because they allow stiffness to be varied at different joints independently. Figs.3.2 and 3.3, show the pulley-system arrangement for synergy actuation. Pulley radii are in the ratio of joint synergies. i^{th} link is attached to i^{th} pulley via torsional springs of spring constant k_i. Both pulley and link are free to rotate on a common axle. All the pulleys are actuated using the same displacment actuator. In absence of any external force, the finger links rotate by the same degree as the pulley connected to it via spring.

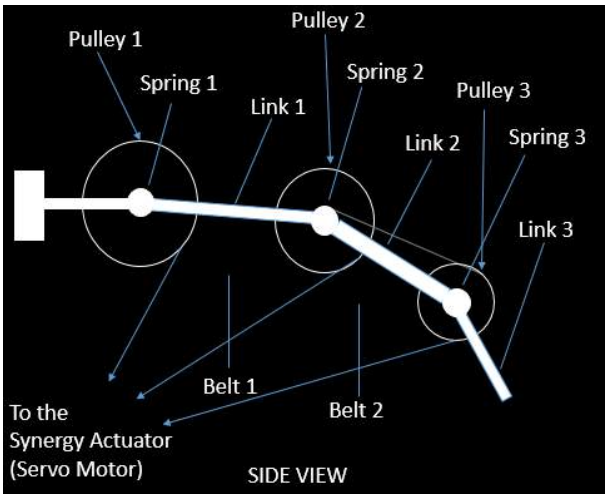

Figure 3.2: Side View of synergy and compliance mechanism.

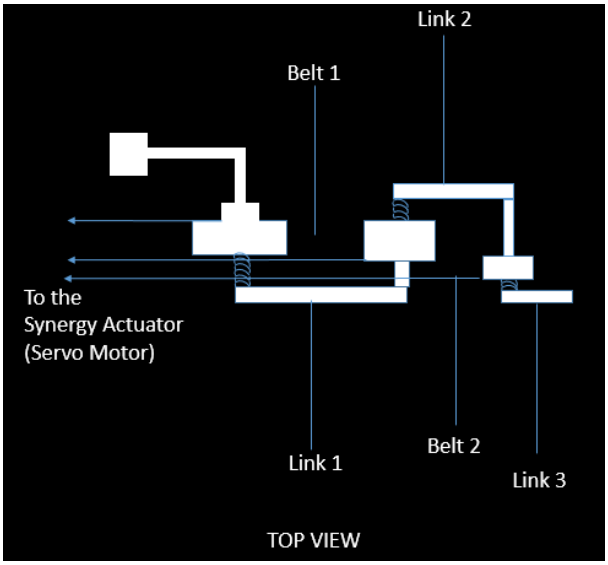

Figure 3.3: Top View of synergy and compliance mechanism.

The stiffness controller mechanism (shown in Fig.3.4), is super-imposed on the synergy structure. Tendons can be routed along the links both on the dorsal and palmar side of the finger. One end of the tendon is fixed on a suitable phalanx at a position which gives the desired moment arm.The stiffness controllers use multi-articular (which pass over multiple joints) tendons routed along the finger (see Fig. 3.4), through which torque (Δ) is transmitted to the joints. Thus actuators can be kept away from the joints, avoiding increase of hand inertia.

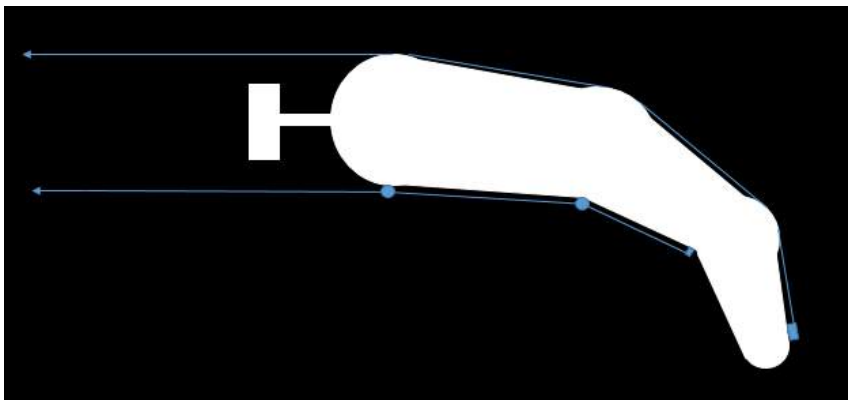

Figure 3.4: Variable compliance mechanism.

The general form of torque matrix (Δ) with 20 joints and m stiffness controllers is as shown.

$$\Delta = \begin{bmatrix} a_{1,1} & a_{1,2} & . & . & . & a_{1,m} \\ a_{2,1} & a_{2,2} & . & . & . & a_{2,m} \\ . & . & . & . & . & . \\ . & . & . & . & . & . \\ a_{20,1} & a_{20,2} & . & . & . & a_{20,m} \end{bmatrix} \begin{bmatrix} T_1 \\ T_2 \\ . \\ . \\ T_m \end{bmatrix} \tag{3.14}$$

Here T_j is the cable tension associated with the j^{th} actuator and $a_{i,j}$ is the moment arm of the T_j on the i^{th} joint. (NOTE: This design is different from adaptive synergy discussed in 3^{rd} chapter. There the synergy parameter σ is force, while here it is displacement.)

3.3.2 Analysis of the structure

From eqn. (3.12) & (3.14), we can see that for two stiffness actuators and three joints the equilibrium equation will be:

$$\begin{bmatrix} \tau_1 \\ \tau_2 \\ \tau_3 \end{bmatrix} = \begin{bmatrix} k_1 & 0 & 0 \\ 0 & k_2 & 0 \\ 0 & 0 & k_3 \end{bmatrix} \begin{bmatrix} \sigma_1 E_{1,1} - q_1 \\ \sigma_1 E_{2,1} - q_2 \\ \sigma_1 E_{3,1} - q_3 \end{bmatrix} + \begin{bmatrix} a_{1,1} & a_{1,2} \\ a_{2,1} & a_{2,2} \\ a_{3,1} & a_{3,2} \end{bmatrix} \begin{bmatrix} T_1 \\ T_2 \end{bmatrix} \tag{3.15}$$

These Torques are balanced by the external forces acting on the finger and equation in notation form is:

$$J^T f = \tau = K \cdot (\sigma_1 E_1 - q) + T_1 a_1 + T_2 a_2 \tag{3.16}$$

Here, $q = \begin{bmatrix} q_1 \\ q_2 \\ q_3 \end{bmatrix}$, $a_j = \begin{bmatrix} a_{1,j} \\ a_{2,j} \\ a_{3,j} \end{bmatrix}$ and $E_k = \begin{bmatrix} E_{1,k} \\ E_{2,k} \\ E_{3,k} \end{bmatrix}$ Further analysis considers the case of force, f_c acting on the fingertip as shown in the figure:
For this case the Jacobian matrix is only a function of q_1, q_2 and q_3 and L.H.S. of eqn. (32) is:

$$J^T(q) f = \begin{bmatrix} f_c L_1 sin(q_2 + q_3 - \beta) + f_c L_2 sin(q_3 - \beta) + f_c L_3 sin(-\beta) \\ f_c L_2 sin(q_3 - \beta) + f_c L_3 sin(-\beta) \\ f_c L_3 sin(-\beta) \end{bmatrix} \tag{3.17}$$

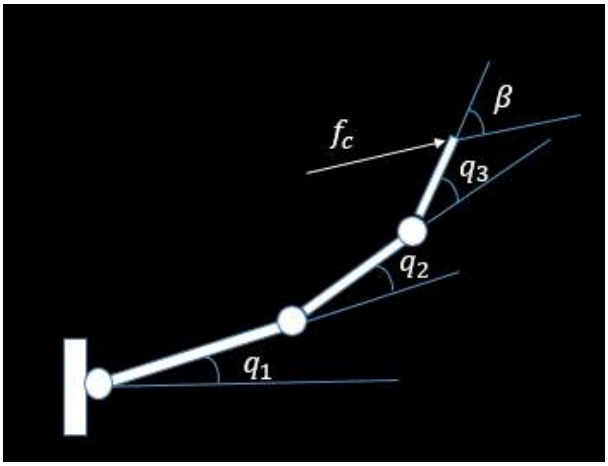

Figure 3.5: Force on the fingertip .

Rearranging the terms, we arrive at following eqn.:

$$\begin{bmatrix} \sigma_1 \\ T_1 \\ T_2 \end{bmatrix} = \begin{bmatrix} k_1 E_{1,1} & a_{1,1} & a_{1,2} \\ k_2 E_{2,1} & a_{2,1} & a_{2,2} \\ k_3 E_{3,1} & a_{3,1} & a_{3,2} \end{bmatrix}^{-1} \begin{bmatrix} k_1 q_1 + f_c L_1 sin(q_2 + q_3 - \beta) + f_c L_2 sin(q_3 - \beta) + f_c L_3 sin(-\beta) \\ k_2 q_2 + f_c L_2 sin(q_3 - \beta) + f_c L_3 sin(-\beta) \\ k_3 q_3 + f_c L_3 sin(-\beta) \end{bmatrix} \tag{3.18}$$

The LHS of eqn.(3.18) are the input parameters while right hand side is the function of desired output. Using this equation, force generation capabilities (f_c) for different postures (q_1, q_2, q_3) at desired angle of attack (β), can be computed.

3.4 INTERACTION WITH OBJECTS

3.4.1 Case 1 : Soft Object

If a soft object is desired to be held, without compressing it, in a particular pose then $f_c \approx 0$

$\Rightarrow$

$$\begin{bmatrix} \sigma_1 \\ T_1 \\ T_2 \end{bmatrix} = \begin{bmatrix} k_1 E_{1,1} & a_{1,1} & a_{1,2} \\ k_2 E_{2,1} & a_{2,1} & a_{2,2} \\ k_3 E_{3,1} & a_{3,1} & a_{3,2} \end{bmatrix}^{-1} \begin{bmatrix} k_1 q_1 \\ k_2 q_2 \\ k_3 q_3 \end{bmatrix} \tag{3.19}$$

So the system can hold the object in any desired pose. Same is true for finger motion in free space. However the whole hand can still be underactuated (See the section on scalability of design to whole hand in future work), as all degrees of freedom can't be independently controlled.

If we consider the case where object is assumed to compress, then during the time of approach any posture can be fixed (assuming it makes contact). Then the further changes in posture and force can be determined from eqn (3.18) using its differential form and the object stiffness properties in the direction corresponding to β angle of attack:

3.4.2 Case 2 : Rigid Object

In case of rigid objects, the posture can be decided during approach. Then, fixing the posture i.e. $\delta q_i = 0$, where i = 1,2,3 $\Rightarrow$

$$\begin{bmatrix} \delta\sigma_1 \\ \delta T_1 \\ \delta T_2 \end{bmatrix} = \begin{bmatrix} k_1E_{1,1} & a_{1,1} & a_{1,2} \\ k_2E_{2,1} & a_{2,1} & a_{2,2} \\ k_3E_{3,1} & a_{3,1} & a_{3,2} \end{bmatrix}^{-1} \delta f_c \begin{bmatrix} -(L_1sin(\beta-q_2-q_3)+L_2sin(\beta-q_3)+L_3sin(\beta)) \\ -(L_2sin(\beta-q_3)+L_3sin(\beta)) \\ -L_3sin(\beta) \end{bmatrix} \tag{3.20}$$

Hence, σ_1, T_1, T_2 can be varied in the fixed ratio of $(L_1sin(\beta-q_2-q_3)+L_2sin(\beta-q_3)+L_3sin(\beta)) : (L_2sin(\beta-q_3)+L_3sin(\beta)) : L_3sin(\beta)$, respectively to achieve the desired force change.

3.4.3 Interaction with object of Stiffness K_0

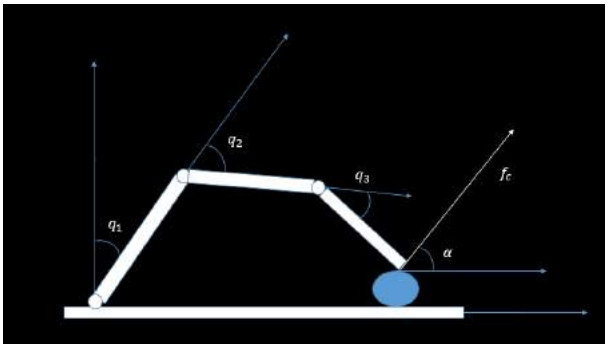

Figure 3.6: Interaction with object of Stiffness K_0.

Fig. 3.6 shows the interaction. The finger is in contact with the object such that force f_c on the finger is at an angle α with the horizontal. For the sake of simplicity of equations let's assume that lengths of links are equal. Then, equations for interaction turn out to be as

follows:

$$\begin{bmatrix} k_1E_{1,1} & a_{1,1} & a_{1,2} \\ k_2E_{2,1} & a_{2,1} & a_{2,2} \\ k_3E_{3,1} & a_{3,1} & a_{3,2} \end{bmatrix} \begin{bmatrix} \sigma_1 \\ T_1 \\ T_2 \end{bmatrix} = \begin{bmatrix} k_1q_1 \\ k_2q_2 \\ k_3q_3 \end{bmatrix} + f_cL \begin{bmatrix} cos(q_1+\alpha)+cos(q_1+q_2+\alpha)+cos(q_1+q_2+q_3+\alpha) \\ cos(q_1+q_2+\alpha)+cos(q_1+q_2+q_3+\alpha) \\ cos(q_1+q_2+q_3+\alpha) \end{bmatrix} \tag{3.21}$$

Let,

$$cos(q_1+\alpha)+cos(q_1+q_2+\alpha)+cos(q_1+q_2+q_3+\alpha) = Q_1$$

$$cos(q_1+q_2+\alpha)+cos(q_1+q_2+q_3+\alpha) = Q_2$$

$$cos(q_1+q_2+q_3+\alpha) = Q_3$$

In differential form this becomes:

$$\begin{bmatrix} k_1E_{1,1} & a_{1,1} & a_{1,2} \\ k_2E_{2,1} & a_{2,1} & a_{2,2} \\ k_3E_{3,1} & a_{3,1} & a_{3,2} \end{bmatrix} \begin{bmatrix} \delta\sigma_1 \\ \delta T_1 \\ \delta T_2 \end{bmatrix} = \begin{bmatrix} k_1\delta q_1 \\ k_2\delta q_2 \\ k_3\delta q_3 \end{bmatrix} + L \begin{bmatrix} Q_1 \\ Q_2 \\ Q_3 \end{bmatrix} \delta f_c + f_cL \begin{bmatrix} \delta Q_1 \\ \delta Q_2 \\ \delta Q_3 \end{bmatrix} \tag{3.22}$$

and

$$\delta f_c = LK_0(Q_1\delta q_1 + Q_2\delta q_2 + Q_3\delta q_3) \tag{3.23}$$

Eqn (3.23) comes from the object stiffness relation. Object stiffness in the direction of force f_c is K_0 and the component of displacement in the direction of force is $L(Q_1\delta q_1+Q_2\delta q_2+Q_3\delta q_3)$. Substituting the values of Q_1, Q_2, Q_3 and δf_c in eqn (3.22), we get

$$\begin{bmatrix} \delta\sigma_1 \\ \delta T_1 \\ \delta T_2 \end{bmatrix} = \begin{bmatrix} k_1E_{1,1} & a_{1,1} & a_{1,2} \\ k_2E_{2,1} & a_{2,1} & a_{2,2} \\ k_3E_{3,1} & a_{3,1} & a_{3,2} \end{bmatrix}^{-1} \begin{bmatrix} X & U & V \\ U & Y & W \\ V & W & Z \end{bmatrix} \begin{bmatrix} \delta q_1 \\ \delta q_1 \\ \delta q_2 \end{bmatrix} \tag{3.24}$$

Where,

$$X = K_0L^2Q_1^2 - Lf_cA + k_1\,, \qquad Y = K_0L^2Q_2^2 - Lf_cB + k_2 \qquad \text{and} \qquad Z = K_0L^2Q_3^2 - Lf_cC + k_3$$

$$U = K_0L^2Q_1Q_2 - Lf_cB\,, \qquad V = K_0L^2Q_1Q_3 - Lf_cC \qquad \text{and} \qquad W = K_0L^2Q_2Q_3 - Lf_cC$$

$$A = sin(q_1+\alpha)+sin(q_1+q_2+\alpha)+sin(q_1+q_2+q_3+\alpha)$$

$$B = sin(q_1+q_2+\alpha)+sin(q_1+q_2+q_3+\alpha) = Q_2$$

$$C = sin(q_1 + q_2 + q_3 + \alpha)$$

This shows that multiple desired finger postures can be achieved, for any given force. Hence the hand essentially simulates variable stiffness. The final finger posture and force is determined by equilibrium between finger-stiffness and object-stiffness.

3.5 IMPLEMENTATION OF DESIGN

3.5.1 Design Specifications

In our case, PCA reveals that $E_{1,1} : E_{2,1} : E_{3,1} = 265 : 222 : 155$. This is used to determine the radii of pulleys. Setting $R_3 = 1$cm $\rightarrow R_2 = 1.43$ cm and $R_3 = 1.71$ cm.
Stiffness values k_1, k_2, k_3 are supposed to be high enough so that system is response is fast. Stiffness value can't be too high because, as they determine the stiffness of 'soft' state of the hand. The minimum stiffness is chosen based on settling time from dynamic response curve. For $k_1 = 0.01$ Nm/rad, $k_2 = 0.01 Nm/rad$, $k_3 = 0.01$ Nm/rad. Settling time was close to 0.04 sec for as high as 1 rad/sec. A viscous damping of 0.0001 Nm-sec/rad is considered for simulation purposes.
Column vectors a_1 and a_2 can be anything as long as they satisfy the constraint $a_1 \neq a_2$. A better estimate for their values would be made from the prototype. Since T_1 and T_2 can be thought of as 2^{nd} and 3^{rd} synergies, a_1 and a_2 can be chosen such that $a_1 = E_2$ and $a_2 = E3$. In this case, there would be 1 displacement synergy (σ_1) and 2 force synergies (T_1 and T_2). This could be crucial in human hand like dexterous manipulation.

3.5.2 First Synergy Implementation

The first synergy implementation (Fig. 3.7) on a single finger consists of three equal pulleys, each of diameter 2 cm which a semi-circular channel in the pulley (Fig. 3.8a) that houses two linear extension springs.
One end of the each spring is fixed to the end of the channel on the pulley. Another end of the spring is attached to a small rod. This rod (parallel to axis of the pulley) passes through the small holes (Fig. 3.8b) on the two parallel link on the opposite sides of the pulley on the common axis. This small rod couples the links and the pulley via the spring.
Three separate cables are passed over each pulley and wrapped over a drum (Fig. 3.9) with three pulley which have diameters in the ratio of first synergy.It is necessary to pass the cable from outer pulleys on the finger (pulley 3 and 2) through the axes of inner pulleys on the

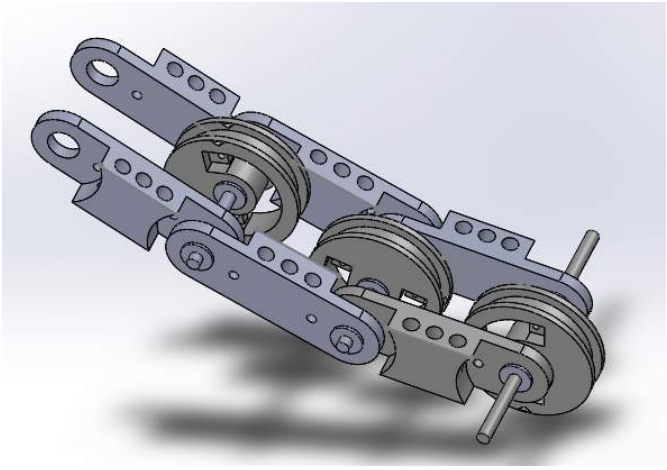

Figure 3.7: First synergy implementation.

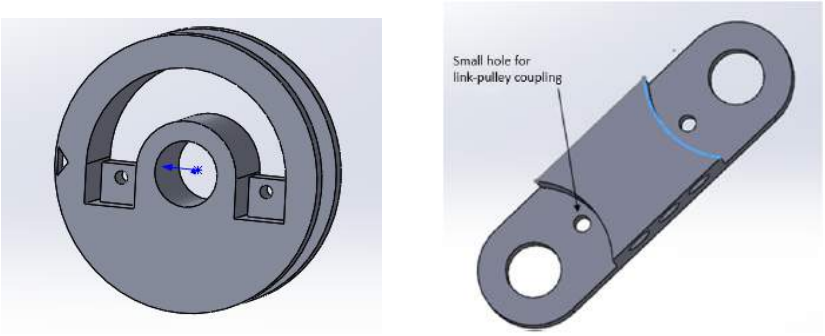

(a) Pulley Design. **(b)** Link Design.

Figure 3.8

finger (pulley 1 and 2 for pulley 3 cable and pulley 1 for pulley 2 cable). This is so that cable from outer pulley don't exert additional torque at inner joints and the equations discussed in the previous sections are maintained.

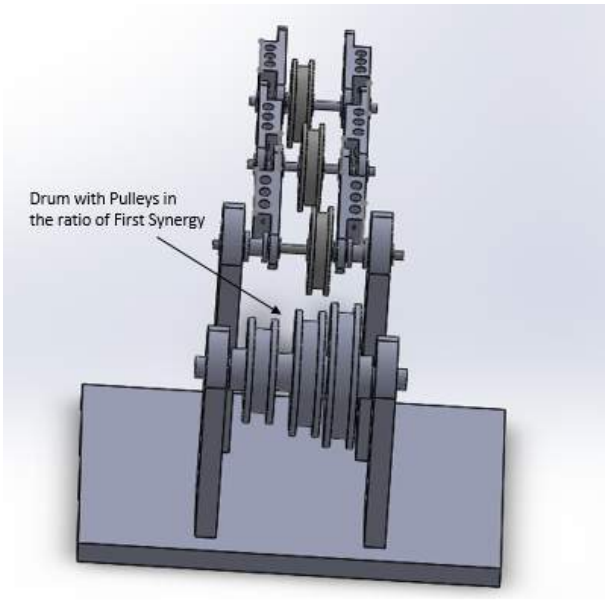

Figure 3.9: First synergy implementation.

3.5.3 Implementation of Variable Stiffness Actuation

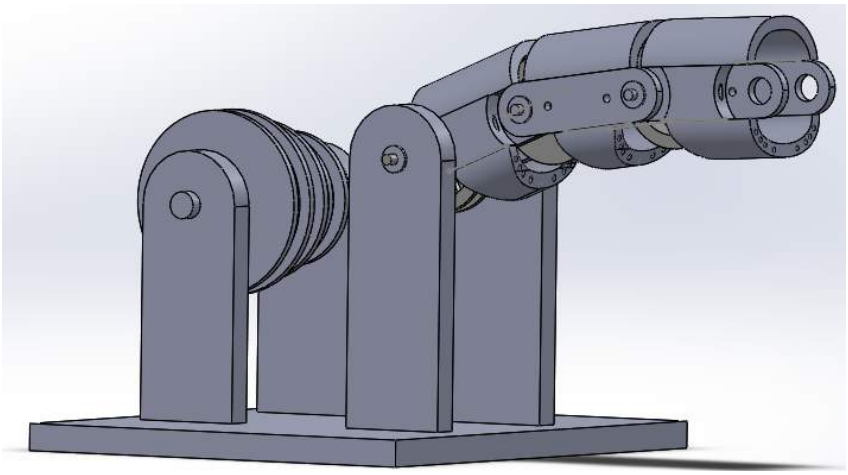

Figure 3.10: Variable Stiffness Implementation.

The Variable Stiffness mechanism is superimposed over the first synergy mechanism. Two outer shells (Fig.3.11) are attached to the link using plug-socket joint. These shells have holes in them to route the variable stiffness tendons, which are then connected to the force source.

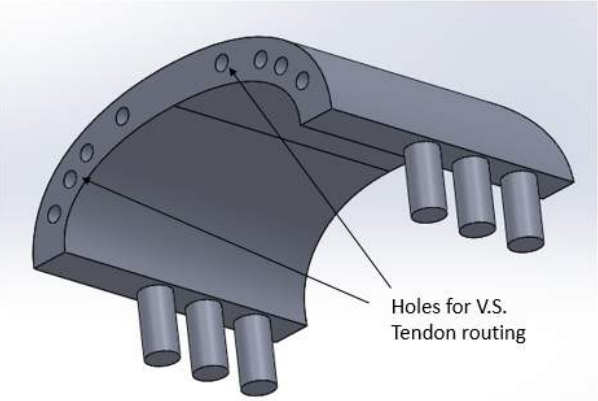

Figure 3.11: Shell with tendon routes.

3.6 SUMMARY

In this chapter we presented a conceptual design of the finger which consisted of three joints actuated by three actuator: one displacment actuator and two force actuator. We also analysed the control structure of the finger, which allows us to determine each actuation parameters explicitly as a function of desired output posture. We further studied some cases of object interaction with the finger. In next chapter, we present some of the simulations highlighting the capabilities of the finger.

Chapter 4

Results and discussion

4.1 SIMULATIONS

Dynamics of the finger links is governed by following equations:

$$M\begin{bmatrix}\ddot{q}_1\\ \ddot{q}_2\\ \ddot{q}_3\end{bmatrix}+C\begin{bmatrix}\sum_{i=1}^{2}\dot{q}_i * \sum_{i=1}^{3}\dot{q}_j\\ \sum_{i=1}^{2}\dot{q}_i * \sum_{i=1}^{3}\dot{q}_j\\ \sum_{i=1}^{2}\dot{q}_i * \sum_{i=1}^{3}\dot{q}_j\end{bmatrix}+\beta\begin{bmatrix}\dot{q}_1\\ \dot{q}_2\\ \dot{q}_3\end{bmatrix}=\begin{bmatrix}\tau_1\\ \tau_2\\ \tau_3\end{bmatrix} \tag{4.1}$$

where $\begin{bmatrix}\tau_1\\ \tau_2\\ \tau_3\end{bmatrix} = J^T f_{ext} + \tau_{actuators}$ and $\tau_{actuators} = \begin{bmatrix}k_1E_{1,1} & a_{1,1} & a_{1,2}\\ k_2E_{2,1} & a_{2,1} & a_{2,2}\\ k_3E_{3,1} & a_{3,1} & a_{3,2}\end{bmatrix}\begin{bmatrix}\sigma_1\\ T_1\\ T_2\end{bmatrix}$

4.1.1 Displacement Mode/First Synergy Actuation

In this simulation, the dynamic response of the finger is determined in response to sinusoidal input at the displacement actuator. The dynamics is given in eqn.(4.1), where $f_{ext} = 0$, $T_1 = 0$ and $T_2 = 0$. Response is determined for two sinusoidal inputs: $\sigma = \sin 10\pi t$ (5 Hz) and $\sigma = \sin 2\pi t$ (1 Hz). 5 Hz is the peak operational frequency of the human hand. The response for $\sigma = \sin 10\pi t$ is shown in Fig. 4.1. The finger isn't able to follow the desired synergy ratio at this frequency.

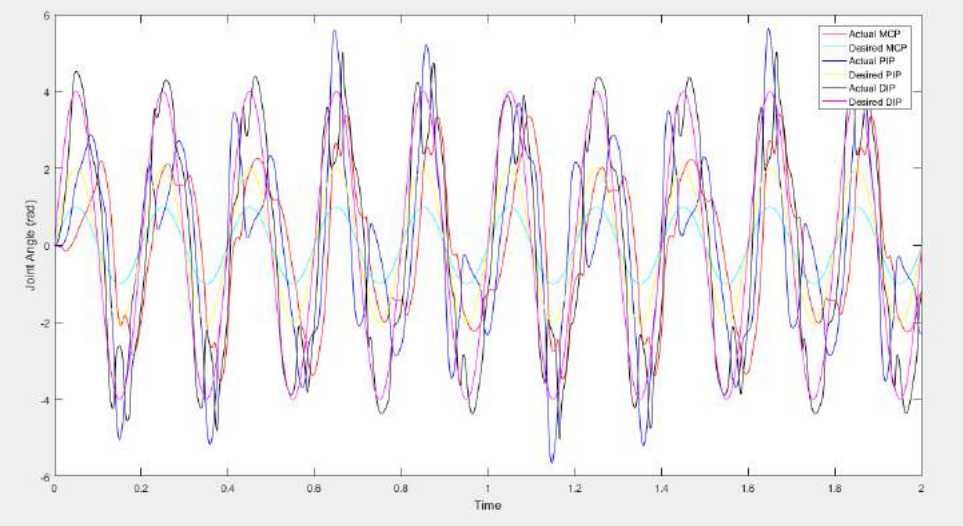

Figure 4.1: Displacement Mode Setup

The response for $\sigma = \sin 2\pi t$ is shown in Fig. 4.2. From this figure we can see that the finger can output the desired ratio of joint anglescfor lower frequencies.

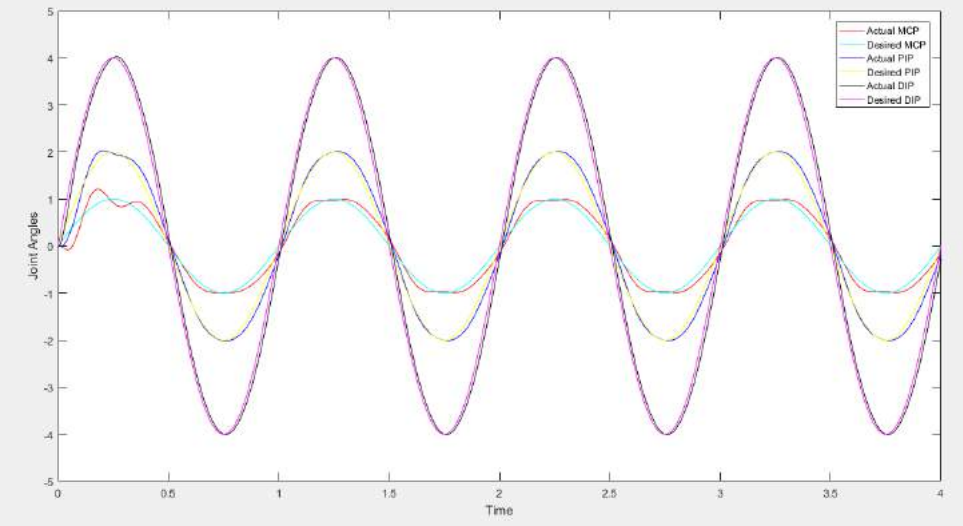

Figure 4.2: Displacement Mode Setup

4.1.2 Trajectory Tracking

This simulation is done to demonstrate the ability of finger to follow any desired trajectory for each joint independent of each other. From eqn.(4.5) we can determine the actuation parameters σ, T1 and T2, by setting K_X and K_Y equal to 0 and q_1, q_2 and q_3 to the desired

trajectory.(Note: This is open loop control.) Thus,

$$\begin{bmatrix} \sigma_1 \\ T_1 \\ T_2 \end{bmatrix} = K^{-1} \begin{bmatrix} k_1 q_{1,des} \\ k_2 q_{2,des} \\ k_3 q_{3,des} \end{bmatrix} \tag{4.2}$$

In the following simulation, we gave sinusoidal input $q_{1,des} = 1 + \sin(pit)$, $q_{2,des} = 1 + 0.5\sin(pit)$ and $q_{3,des} = 1 + \sin(pi/2t)$. The resulting trajectory of the finger is shown in Fig. 4.3. The finger is able to follow the desired trajectory.

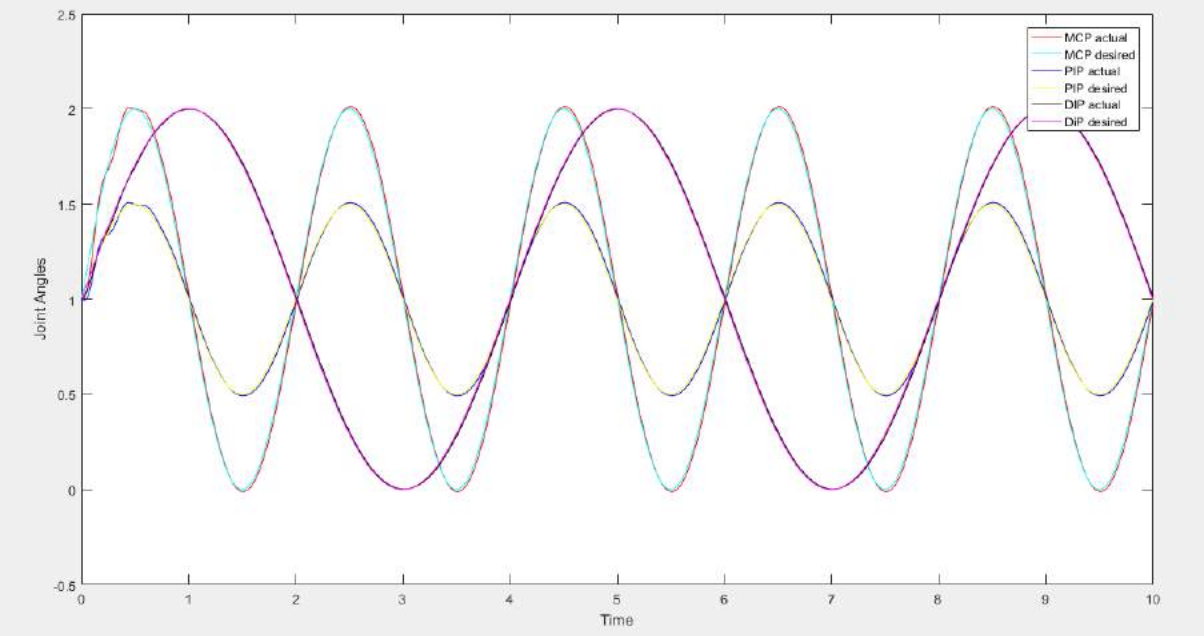

Figure 4.3: Trajectory tracking.

4.1.3 First Synergy Actuation with wall collision

As shown in Fig. 4.4, the finger base and the horizontal surface are fixed. The finger is initially horizontal and the vertical distance between finger and the surface is 1.5 cm. The wall is modeled as a spring-damper system with stiffness and damping constants as K_{con} and C_{con} respectively. Surface is assumed frictionless and so the contact force along x-direction in zero.The finger is operated using the first synergy motor at a constant rate of 6 rad/min, so the joint angles change in those ratios (Here the synergy ratio is taken to be 1:2:3 for MCP, PIP and DIP respectively) accordingly. The dynamics is given in eqn.(4.1), where $f_{ext} = (K_{con}(y - y_0) + C_{con} * \dot{y}) * u_s(y - y_0)$, $T_1 = 0$ and $T_2 = 0$.The displacement actuator is given an input such that $\sigma = 0.1t$ .When the contact occurs, the finger starts to yield and as

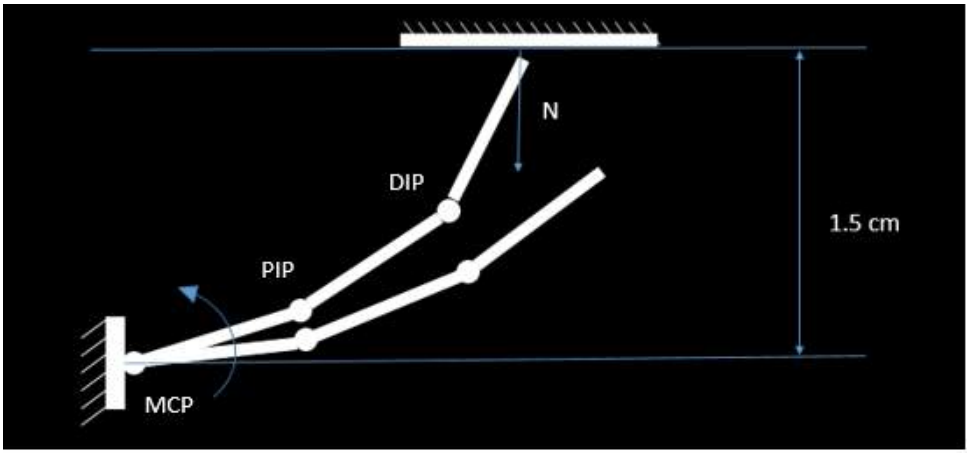

Figure 4.4: Displacement Mode Setup

the synergy actuator is further moved, the normal force starts rising.
Fig. 4.5 and 4.6 show the variation of contact force after contact for wall stiffness 2000 N/m and 100 N/m respectively. Damping constant of the wall is 0.01 N-s/m in both cases.

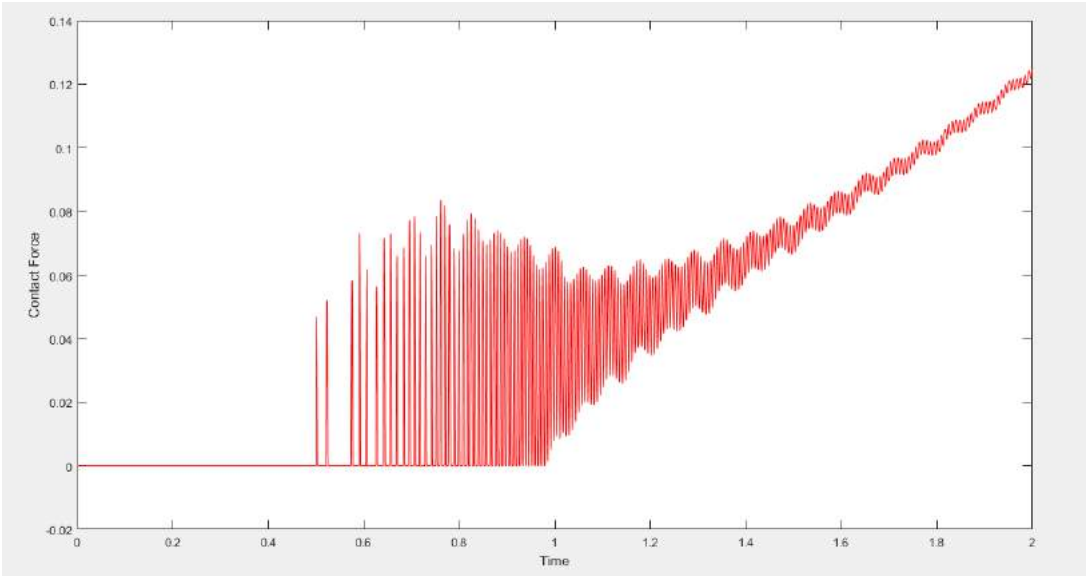

Figure 4.5: Contact Force vs time for displacement mode for wall stiffness $K_{contact}$=2000 N/m

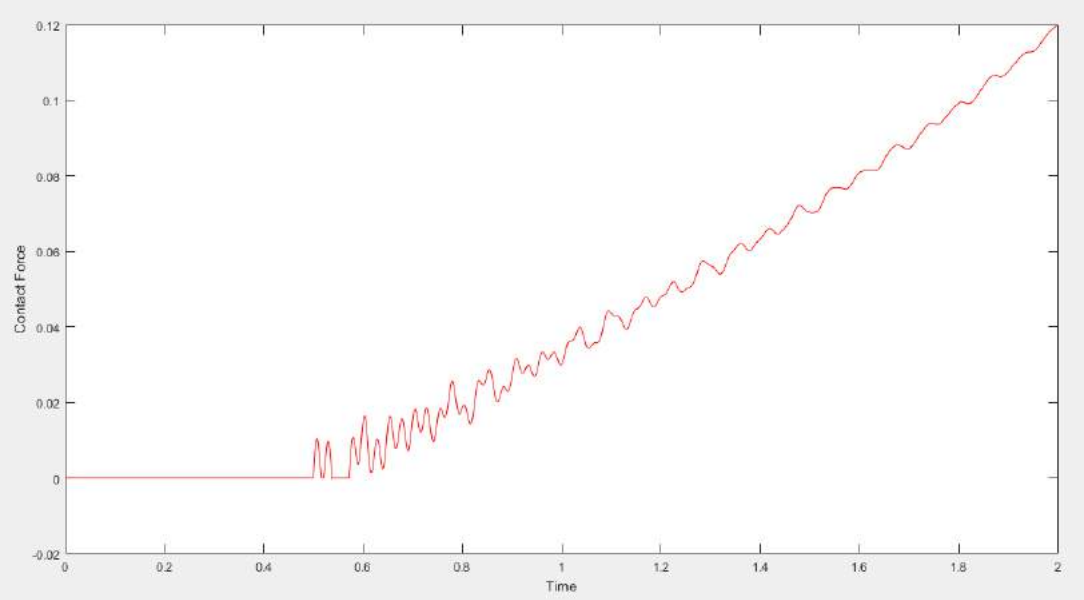

Figure 4.6: Contact Force vs time for displacement mode for wall stiffness $C_{contact}$=100 N/m

The finger moves freely without any external force in accordance with first synergy until contact happens at t=0.5 sec. After contact, the finger starts to yield. For a higher stiffness of the wall, the finger rebounds from the wall and looses contact(Contact Force = 0) at several points of time, before establishing steady contact with increasing contact force as shown in Fig. 4.5. For the softer wall, finger penetrates into the wall maintaining contact and the contact force gradually increases. It is to be noted that there is no actuator torque limit imposed in the simulation. So, the contact force could keep on increasing with increasing finger penetration. In reality, actuator limit will reach at some point and the finger will start sliding along the wall after that.

Fig. 4.7 and 4.8 shows the evolution of finger posture in space for spring constants 2000 N/m and 100 N/m.

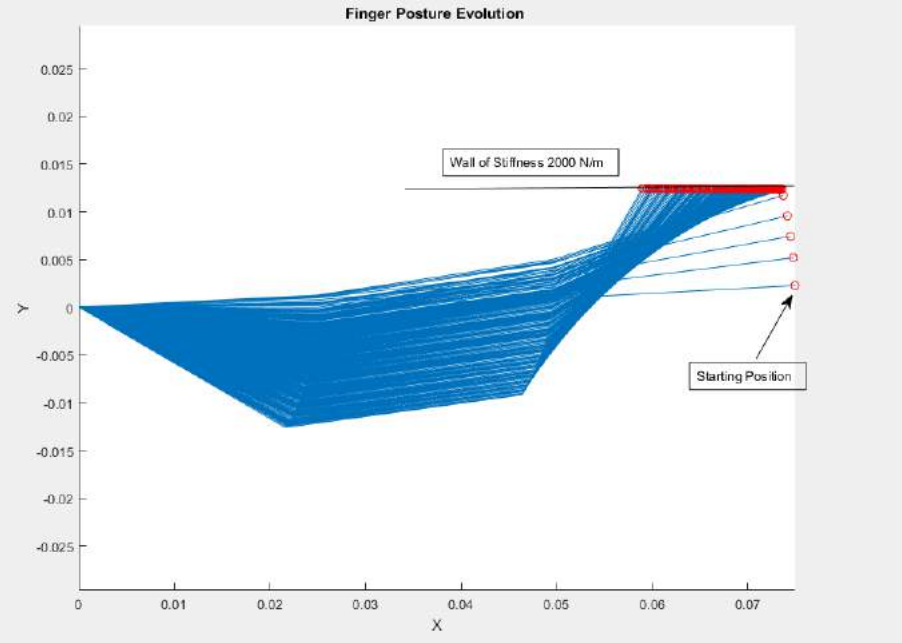

Figure 4.7: Finger Posture evolution for displacement mode

As shown in Fig. 4.7, the penetration of finger in the wall of stiffness 2000 N/m is very low while for the softer wall shown in Fig. 4.8, there is higher penetration.

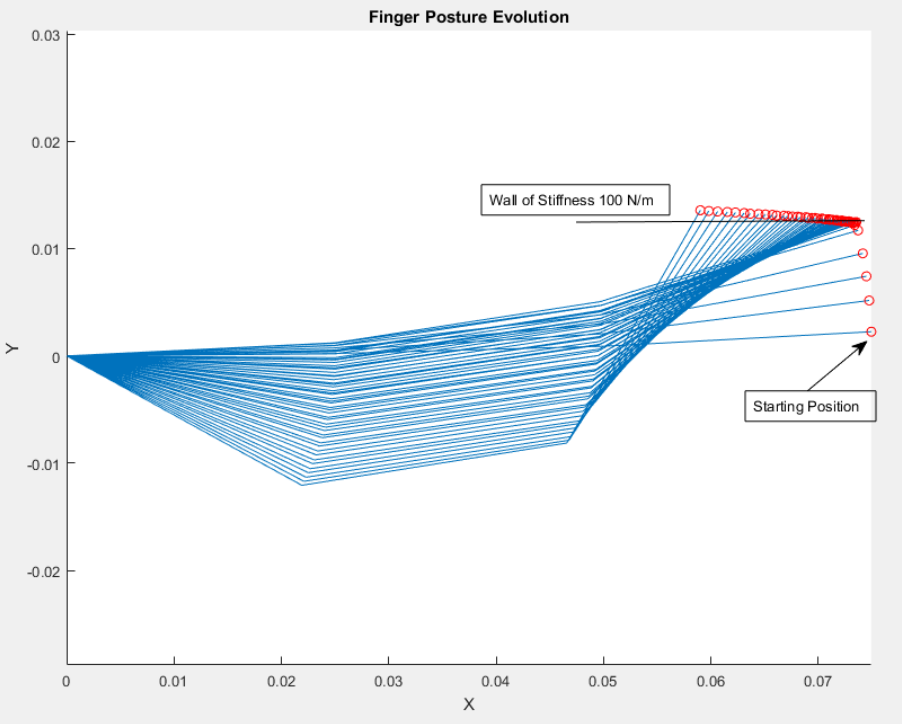

Figure 4.8: Finger Posture evolution for displacement mode

4.1.4 End-point Impedance Control

Simulations were performed to demonstrate the ability of the finger to operate under impedance control.Given a starting posture of finger, if an external force is applied to it, the deflection of the fingertip is determined by the desired resultant stiffness at the endpoint. An open loop impedance controller is used for this purpose. Here, we simulate the dynamics of the finger for a step force input and a ramp input. The dynamics of the finger links is given by eqn. of the following form

$$M \begin{bmatrix} \ddot{q}_1 \\ \ddot{q}_2 \\ \ddot{q}_3 \end{bmatrix} + C \begin{bmatrix} \sum_{i=1}^{2} \dot{q}_i * \sum_{i=1}^{3} \dot{q}_j \\ \sum_{i=1}^{2} \dot{q}_i * \sum_{i=1}^{3} \dot{q}_j \\ \sum_{i=1}^{2} \dot{q}_i * \sum_{i=1}^{3} \dot{q}_j \end{bmatrix} + \beta \begin{bmatrix} \dot{q}_1 \\ \dot{q}_2 \\ \dot{q}_3 \end{bmatrix} = \begin{bmatrix} \tau_1 \\ \tau_2 \\ \tau_3 \end{bmatrix} \tag{4.3}$$

where $$\begin{bmatrix} \tau_1 \\ \tau_2 \\ \tau_3 \end{bmatrix} = J^T f_{ext} + \tau_{actuators}$$

We want to simulate the behavior such that under quasi-static condition finger deflection from initial position in x-direction $\Delta X = f_{eX}/K_X$, where K_X and f_{eX} are desired stiffness and external force in x-direction. Hence, under equilibrium

$$J^T \begin{bmatrix} K_X \Delta X \\ K_Y \Delta Y \end{bmatrix} + \tau_{actuators} = 0 \tag{4.4}$$

where $$\tau_{actuators} = \begin{bmatrix} k_1 & 0 & 0 \\ 0 & k_2 & 0 \\ 0 & 0 & k_3 \end{bmatrix} \begin{bmatrix} \sigma_1 E_{1,1} - q_1 \\ \sigma_1 E_{2,1} - q_2 \\ \sigma_1 E_{3,1} - q_3 \end{bmatrix} + \begin{bmatrix} a_{1,1} & a_{1,2} \\ a_{2,1} & a_{2,2} \\ a_{3,1} & a_{3,2} \end{bmatrix} \begin{bmatrix} T_1 \\ T_2 \end{bmatrix}$$

Thus we can determine actuation parameters from the following equation:

$$\begin{bmatrix} \sigma_1 \\ T_1 \\ T_2 \end{bmatrix} = K^{-1} \begin{bmatrix} k_1 q_1 \\ k_2 q_2 \\ k_3 q_3 \end{bmatrix} - K^{-1} J^T \begin{bmatrix} K_X (X - X_0) + C_X \dot{X} \\ K_Y (Y - Y_0) + C_Y \dot{Y} \end{bmatrix} \tag{4.5}$$

where $$K = \begin{bmatrix} k_1 E_{1,1} & a_{1,1} & a_{1,2} \\ k_2 E_{2,1} & a_{2,1} & a_{2,2} \\ k_3 E_{3,1} & a_{3,1} & a_{3,2} \end{bmatrix}$$

(X,Y) and $(\dot{X}, \dot{Y})$ are end point coordinate and velocities respectively. We have introduced

damping to account for oscillations and reduce settling time.

4.1.4.1 Step Force Input

For the simulation $F_{eX} = 1$ N, $F_{eY} = 0$ N, $K_X = 100$ N/m, $K_Y = 10000$ N/m, $C_X = 1$ N-s/m, $C_Y = 1$ N-s/m. The results are shown in Fig.4.9 and 4.10.

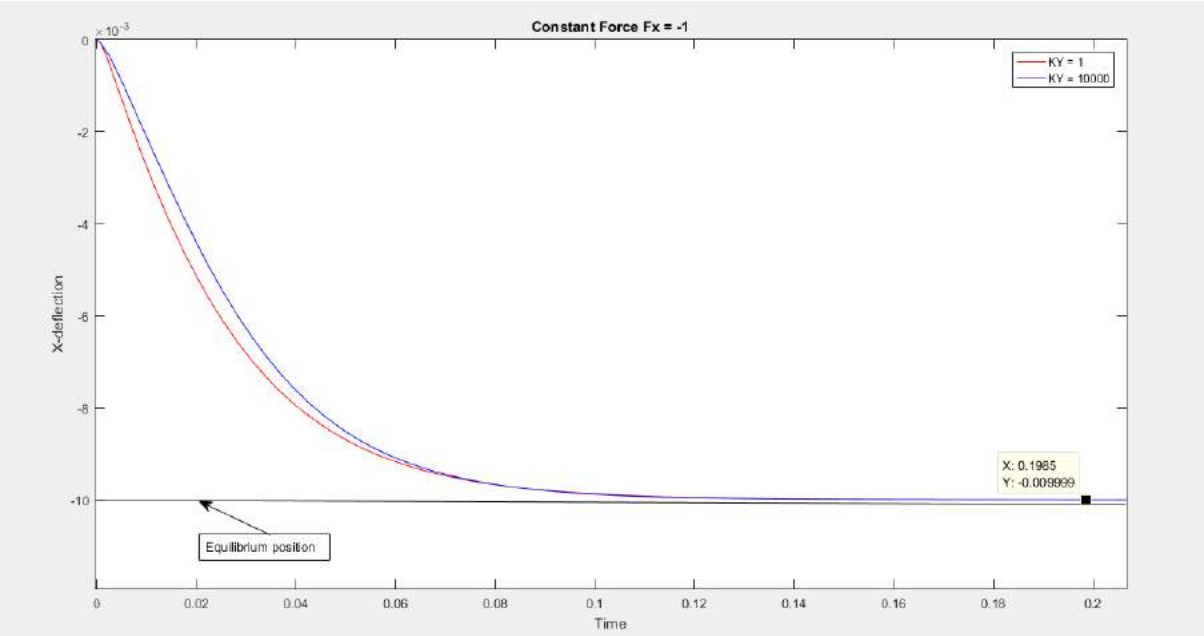

Figure 4.9: X-deflection vs time for Step Force function.

For step force input in x-direction with very high controller stiffness in y-direction should allow finger end-point to move in x-direction such that it settles at F_{eX}/K_X. For low controller stiffness along y-direction, high overshoot happens in y-direction but the end point finally settles at the desired position.

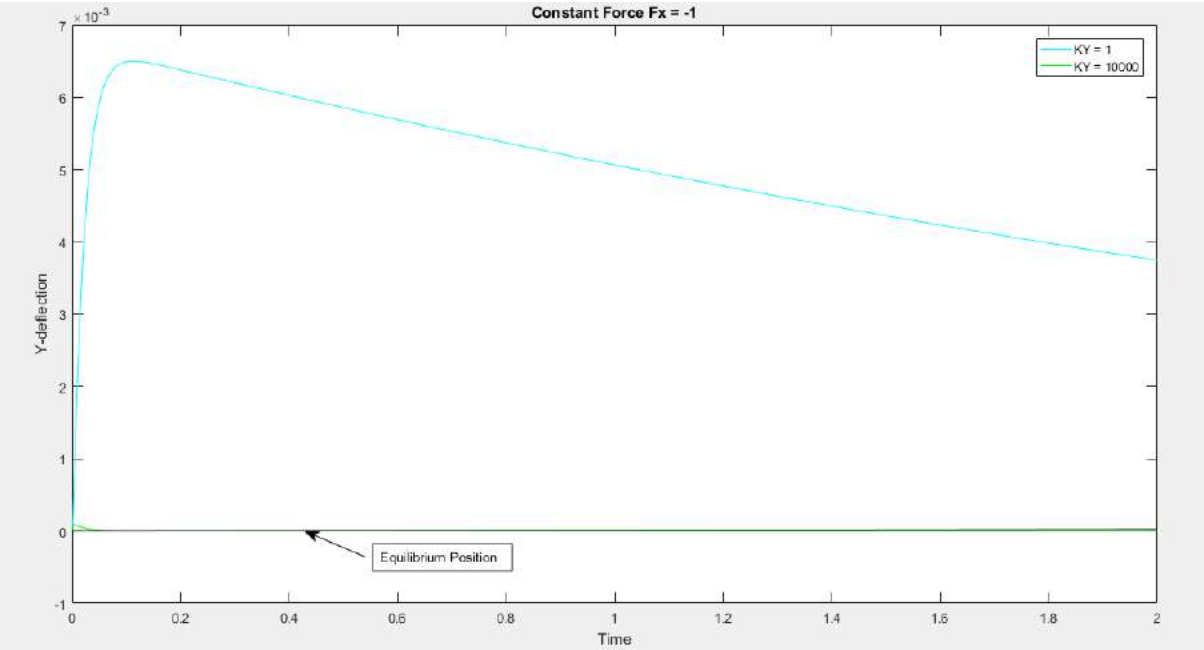

Figure 4.10: Y-deflection vs time for Step Force function.

4.1.4.2 Ramp Force Input

For the simulation $F_{eX} = 0.5t$ N, $F_{eY} = 0$ N, $K_X = 100$ N/m, $K_Y = 10000$ N/m, $C_X = 1$ N-s/m, $C_Y = 1$ N-s/m. The results are shown in Fig.4.11 and 4.12

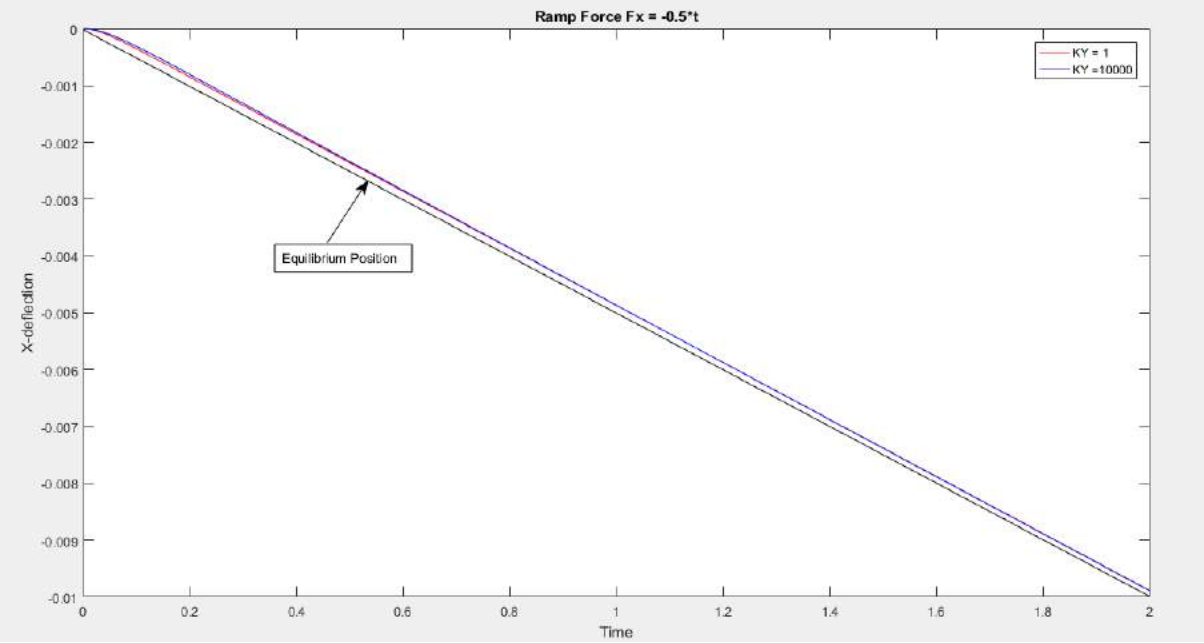

Figure 4.11: X-deflection vs time for Ramp Force function.

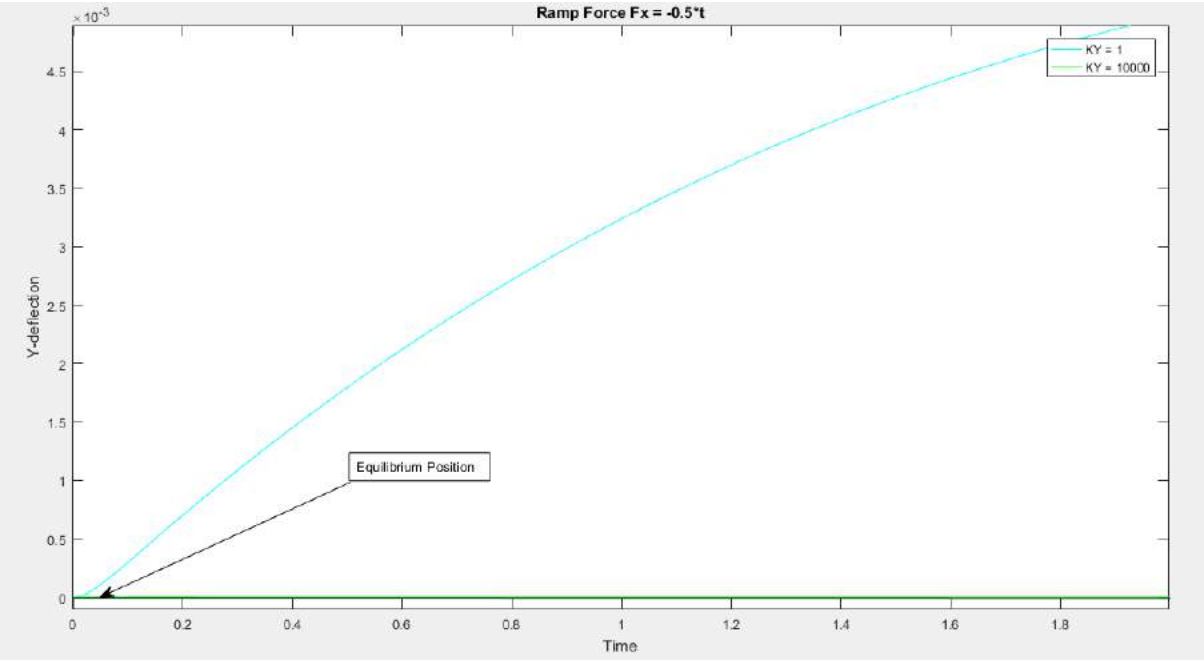

Figure 4.12: Y-deflection vs time for Ramp Force function.

For ramp force input results are as expected, better than in case of step force input with lower overshoot in y-direction even for lower controller stiffness in y-direction.
It is to be noted that the values of T_1 and T_2 are at times required to be negative in order to be able to any possible external force. This requires cables to be on both the palmer as well as dorsal side. Cables from both the sides can be actuated using independent actuators for both. This would double the number of variable stiffness actuators. Another way to accomplish this without increasing the number of actuators is using a clutch based mechanism, such that when one cable(say on the palmer side) is under tension, the opposite one(on the dorsal side) is free.

4.1.5 Disturbance Rejection

In this simulation the open loop controller described in previous section is tested for its ability to handle disturbances in the direction, perpendicular to the direction in which spring behavior is simulated. A constant force of 1 N is applied in negative x-direction and at 0.5 seconds an impulse of 0.01 N-sec acts in positive y-direction. The results are shown for high y-direction stiffness vs low y-direction stiffness, in Figs. 4.13 and 4.14.

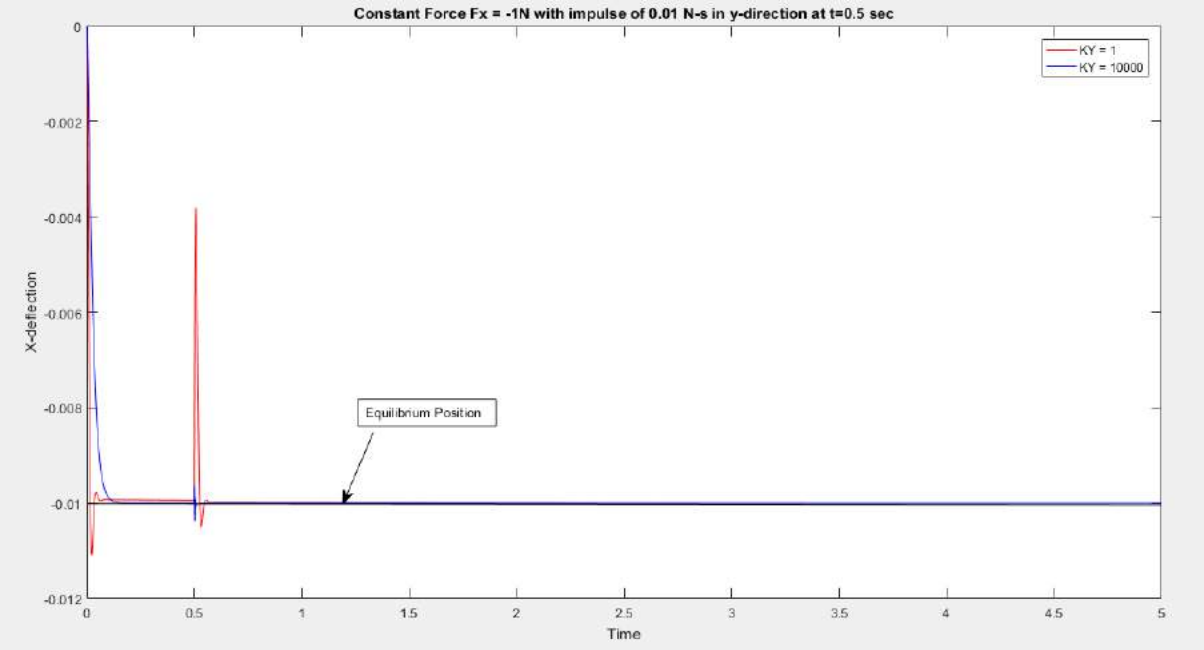

Figure 4.13: X-deflection vs time for Step Force function with impulse of 0.01 N-sec at 0.5 sec.

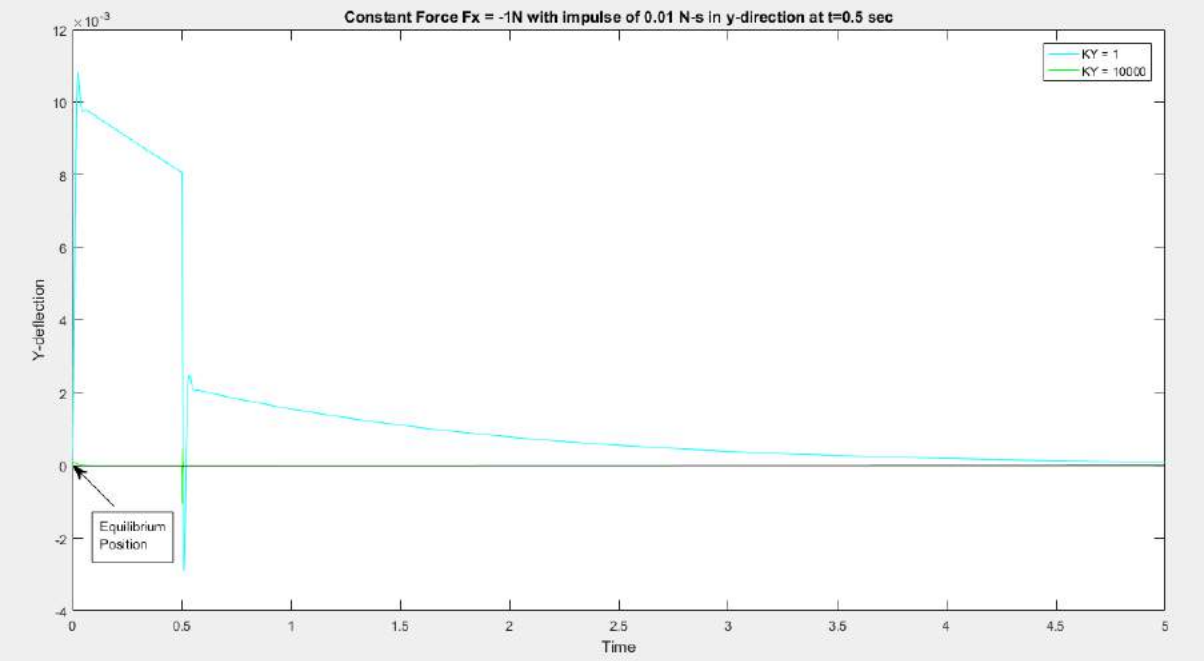

Figure 4.14: Y-deflection vs time for Step Force function with impulse of 0.01 N-sec at 0.5 sec.

As shown in Fig. 4.14 for low stiffness in y-direction, $K_Y = 1$, the finger deflects in the y-direction, while maintaining the desired behavior in the x-direction for most of the time as shown in Fig. 4.13. Thus for a low y-stiffness, behavior in x-direction can be maintained

without reaching the actuator limit. While in case of high y-stiffness, an impulse in y-direction would lead to high actuator torques which could damage the actuator.

4.2 EXPERIMENTS

In this section we present three sets of experiments that were conducted with the finger with a palm attached to the setup.

4.2.1 Free motion using first synergy/displacement actuator

The first synergy actuator was manually operated by rotating the drum. Fig. 4.15 shows the resulting pose of the finger. The objective was to test the output ratio of joint angles as a result of first synergy actuation.

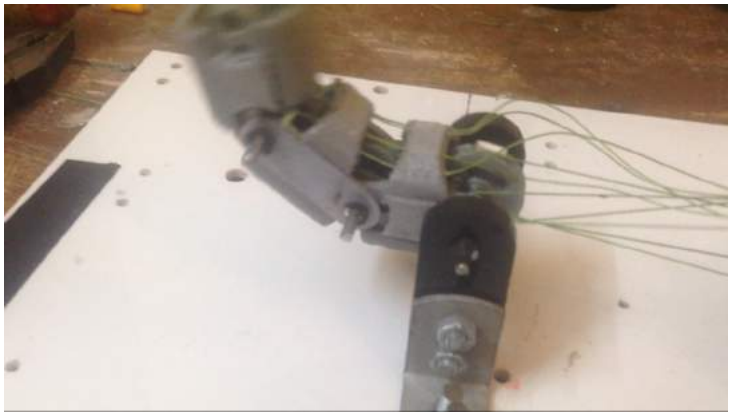

(a)

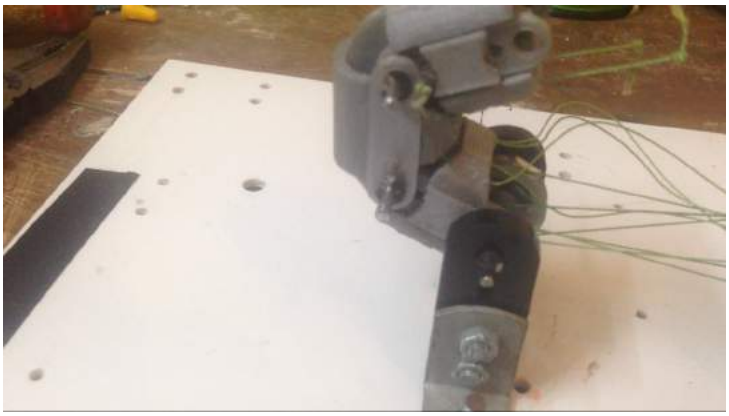

(b)

Figure 4.15: Free Motion using first synergy actuator

4.2.2 Tracking Surfaces of Large objects

The finger is able to conform as a result of contact and can slide along the surface of a large flat, convex or concave objects. Few such experiment is shown in Fig. 4.16 and 4.17. The videos of these experiments are attached along with the file.

(a) **(b)**

Figure 4.16: Convex Surface Tracking

(a)

(b)

Figure 4.17: Flat Surface Tracking

4.2.3 Gripping of objects with different shapes

The finger is able to conform to the surface of several objects and grip them against the surface of the palm and can lift very light objects like marker, a wooden block, a wooden thin strip, pencil etc. Some of these are shown in Fig. 4.18c, 4.19a and 4.19b. (Note: These experiments are conducted using only the displacement actuator)

(a) A wooden block **(b)** A wooden thin strip

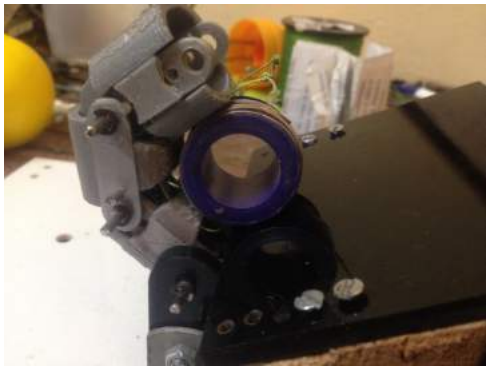

(c) Small Spool

Figure 4.18: Grip of some object

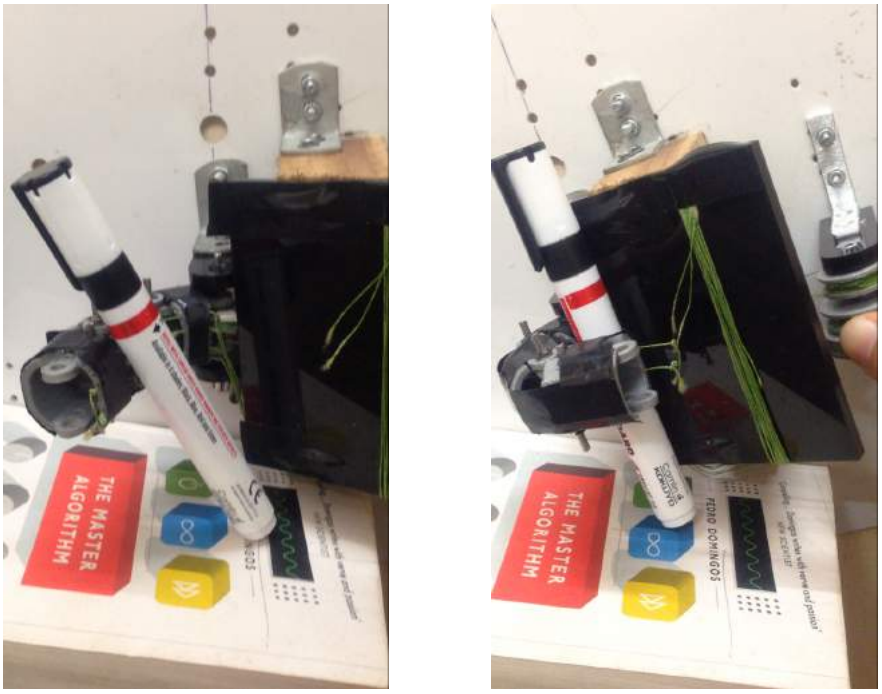

(a) **(b)**

Figure 4.19: Holding a Marker

(a) **(b)**

Figure 4.20: Holding a Spool

4.3 SUMMARY

The finger is able to perform a free motion in accordance with the desired ratio of joint angles as described by the first synergy. Further the finger is also able to conform to a surface and track it just by actuating the first synergy. There are however some discontinuities in motion as spring in the channel has deformed at few places. This issue could be resolved with greater care during assembly of the next prototype.

Along with the palm, the finger is able to hold a variety of shapes and sizes and lift light objects. It has trouble in lifting heavy objects however. This is for two reasons. Friction at the finger surface is very low and needs to be addressed by adding friction pads/ soft rubber at the surface. Because of low friction, high normal contact is required to lift a heavy object, which the current prototype is not able to deliver due to lower stiffness of the springs than desired. A custom made spring with desired stiffness needs to be incorporated in the next prototype. Another issue is the length of the finger links. The length of proximal phalanx needs to be increased to increase the hold of the finger over the objects. This would enable it to large objects like white board eraser, spool with greater ease. Also, in order to hold thin objects like pencil with greater ease the fatness of the finger needs to be reduced (for same link lengths). The fingertips need to be thin in order to enable picking of very fine objects like pin. So, in effect the length to fatness ratio of the finger needs to be optimized.

Chapter 5

Conclusion and Future Work

A finger design is presented by using the principle of postural synergies and variable stiffness actuation together. To sum up, synergies are related to motion of finger joints and they offer a way to reduce the degrees of actuation (and hence simplify control) by combining motions of several joints in a single degree of actuation. Thus, only a few degrees of actuation can explain a large variation in the hand postures. Reducing the degrees of actuation also means that some of the hand postures become unattainable. Compliance is introduced to deal with this. This makes hand adaptable to the surface of the objects and increases the range of grasps. Introduction of compliance also offers a way to control the grasp force by relating synergistic motion to grasp forces. However, introduction of compliance means that ability to control the posture is lost, which would make some of the grasps impossible, particularly ones which don't adapt to the shape of the object.This is why variable stiffness mechanism is introduced in the design. This helps better control over grasp forces and hand postures.
The finger design consists of 3 actuators: one synergy actuator and two stiffness controller. The finger is capable of attaining any posture in free space (contact force = 0) The interaction of the finger with both soft and rigid object is discussed in the section 7.3.
Furthermore, the two stiffness actuators which use cables to apply torque at the joints can be made to behave like 2^{nd} and 3^{rd} actuators by choosing the moment arms in the ratio of respective synergies. Through simulations position and impedance control of the finger, using these three actuators, is demonstrated. It is shown that the finger can follow a prescribed trajectory as well as maintain a desired end-point impedance. A prototype of one finger attached to palm was built and a few experiments demonstrating motion of finger in free space and grips of several object with different shapes, were conducted.
In future, experiments related to posture control, trajectory tracking, impedance control and disturbance rejection would be conducted with a new prototype which would have

tendon on both palmer as well as dorsal side of the finger. Each pair actuated through a single actuator with some sort of a clutch. This would allow the finger to implement negative values of stiffness controller variable.
Further the whole hand can be kept underactuated by allowing the same 3 actuators used in a single finger to behave as synergy actuators for the entire hand. Since in the force control equations both displacement actuator as well as force actuator contribute to the torque similarly and are linearly superimposed, they can behave like three synergies provided we implement moment arms of multi-articular tendons appropriately. Thus the whole hand would be underactuated and yet be able to take most of the postures by the virtue of synergy. Another way to keep the hand underactuated is shown in the next section.

Scalability of the design to whole hand

In a human hand, most of the grips that require precision control, involve the index finger, middle finger and thumb (fig.2.1). Ring finger and little finger are mostly involved while performing power grasps which involve conforming to object shape and establishing maximum contact with the surface. So, it is safe to employ variable stiffness tendons only to the former three fingers. Further, the thumb has one less joint. Thus, we can get away with one less stiffness actuator. So, the actuators employed for an entire hand, will be one synergy actuator, two variable stiffness actuators for index and middle finger each and one variable stiffness actuator for the thumb. So, a total of six actuators can be used to control the 20 joints of the hand. Hence the hand is still under-actuated. For the entire hand the design of palm, the abduction-adduction joints, thumb and the opposition function in little finger still needs to be explored, to complete the design of entire hand.

Bibliography

[1] Antonio Bicchi, Michele Bavaro, Gianluca Boccadamo, Davide De Carli, Roberto Filippini, Giorgio Grioli, Marco Piccigallo, Alessandro Rosi, Riccardo Schiavi, Soumen Sen, et al. Physical human-robot interaction: Dependability, safety, and performance. In *Advanced Motion Control, 2008. AMC'08. 10th IEEE International Workshop on*, pages 9–14. IEEE, 2008.

[2] Christopher Y Brown and H Harry Asada. Inter-finger coordination and postural synergies in robot hands via mechanical implementation of principal components analysis. In *Intelligent Robots and Systems, 2007. IROS 2007. IEEE/RSJ International Conference on*, pages 2877–2882. IEEE, 2007.

[3] Manuel G Catalano, Giorgio Grioli, Edoardo Farnioli, Alessandro Serio, Cristina Piazza, and Antonio Bicchi. Adaptive synergies for the design and control of the pisa/iit softhand. *The International Journal of Robotics Research*, 33(5):768–782, 2014.

[4] Manuel G Catalano, Giorgio Grioli, Alessandro Serio, Edoardo Farnioli, Cristina Piazza, and Antonio Bicchi. Adaptive synergies for a humanoid robot hand. In *Humanoid Robots (Humanoids), 2012 12th IEEE-RAS International Conference on*, pages 7–14. IEEE, 2012.

[5] Lei Cui, Ugo Cupcic, and Jian S Dai. An optimization approach to teleoperation of the thumb of a humanoid robot hand: Kinematic mapping and calibration. *Journal of Mechanical Design*, 136(9):091005, 2014.

[6] Mark R Cutkosky. On grasp choice, grasp models, and the design of hands for manufacturing tasks. *IEEE Transactions on robotics and automation*, 5(3):269–279, 1989.

[7] Aaron M Dollar and Robert D Howe. The highly adaptive sdm hand: Design and performance evaluation. *The international journal of robotics research*, 29(5):585–597, 2010.

[8] Clement Gosselin, Frederic Pelletier, and Thierry Laliberte. An anthropomorphic underactuated robotic hand with 15 dofs and a single actuator. In *Robotics and Automation, 2008. ICRA 2008. IEEE International Conference on*, pages 749–754. IEEE, 2008.

[9] Markus Grebenstein, Alin Albu-Schäffer, Thomas Bahls, Maxime Chalon, Oliver Eiberger, Werner Friedl, Robin Gruber, Sami Haddadin, Ulrich Hagn, Robert Haslinger, et al. The dlr hand arm system. In *Robotics and Automation (ICRA), 2011 IEEE International Conference on*, pages 3175–3182. IEEE, 2011.

[10] Victor Petuya, Charles Pinto, and Erwin-Christian Lovasz. *New Advances in Mechanisms, Transmissions and Applications: Proceedings of the Second Conference MeTrApp 2013 p.116*, volume 17. Springer Science & Business Media, 2013.

[11] Rolf Pfeifer and Gabriel Gómez. Morphological computation–connecting brain, body, and environment. *Creating brain-like intelligence*, pages 66–83, 2009.

[12] Aleksandar Rodić, Branko Miloradović, Svemir Popić, Sofija Spasojević, and Branko Karan. Development of modular compliant anthropomorphic robot hand. In *New Trends in Medical and Service Robots*, pages 205–219. Springer, 2014.

[13] Marco Santello, Martha Flanders, and John F Soechting. Postural hand synergies for tool use. *Journal of Neuroscience*, 18(23):10105–10115, 1998.

[14] Pramodsingh H Thakur, Amy J Bastian, and Steven S Hsiao. Multidigit movement synergies of the human hand in an unconstrained haptic exploration task. *Journal of Neuroscience*, 28(6):1271–1281, 2008.

[15] Francisco J Valero-Cuevas, Jae-Woong Yi, Daniel Brown, Robert V McNamara, Chandana Paul, and Hood Lipson. The tendon network of the fingers performs anatomical computation at a macroscopic scale. *IEEE Transactions on Biomedical Engineering*, 54(6):1161–1166, 2007.

[16] Bram Vanderborght, Alin Albu-Schäffer, Antonio Bicchi, Etienne Burdet, Darwin G Caldwell, Raffaella Carloni, M Catalano, Oliver Eiberger, Werner Friedl, Ganesh Ganesh, et al. Variable impedance actuators: A review. *Robotics and autonomous systems*, 61(12):1601–1614, 2013.

[17] Ivan Virgala, Michal Kelemen, and Štefan Mrkva. Kinematic analysis of humanoid robot hand. *American Journal of Mechanical Engineering*, 1(7):443–446, 2013.